UNIVERSITY OF BERGEN
Faculty of Mathematics and Natural Sciences

The linear stationary wave response to Arctic amplification related heating

by

Raymond Sellevold

A thesis submitted in partial fulfillment for the degree of Master of Science
in meteorology and oceanography

in the
Faculty of mathematics and natural sciences
Geophysical institute

June 2015

Declaration of Authorship

I, Raymond Sellevold, declare that this thesis titled, 'The linear stationary wave response to Arctic amplification related heating' and the work presented in it are my own. I confirm that:

- Where any part of this thesis has previously been submitted for a degree or any other qualification at this University or any other institution, this has been clearly stated.
- Where I have consulted the published work of others, this is always clearly attributed.
- Where I have quoted from the work of others, the source is always given. With the exception of such quotations, this thesis is entirely my own work.
- I have acknowledged all main sources of help.
- Where the thesis is based on work done by myself jointly with others, I have made clear exactly what was done by others and what I have contributed myself.

Signed: _____

Date: _____

UNIVERSITY OF BERGEN

Abstract

Faculty of mathematics and natural sciences
Geophysical institute

in meteorology and oceanography

by Raymond Sellevold

There has been a raft of manuscripts which claim to show that Arctic amplification (AA) is responsible for changes in the large-scale wintertime midlatitude atmospheric circulation. Responses to these studies have shown that the results are likely artifacts of the chosen methodology, but do not discount the potential influence of AA on the midlatitude circulation. Few have investigated the physical mechanisms that might link the anomalous heating to midlatitude circulation. In this investigation we employ a linear stationary wave model to investigate the hypothesis that AA, in the form of a low-level anomalous heating of the atmosphere, can drive a midlatitude circulation response. The model is well suited to the question due to its ability to reproduce the observed atmospheric circulation, and its simplicity as it requires only four forcing components plus the zonal mean state from reanalysis. Interpreting the model results is relatively straightforward. The results show that the AA related anomalous heating has a modest direct impact on the midlatitude circulation and a further investigation of possible nonlinear interactions and wave-mean flow interactions are needed.

Acknowledgements

First of all, I would like to thank my supervisors, **Camille Li** and **Stefan Sobolowski**. Thank you for giving me the opportunity to work on such an interesting topic, for all the help you provided me and for many interesting discussions. I have learned so much from you this last year and I am very grateful for this.

Next, I would like to thank **Martin King** for providing me with the diabatic heating. Most likely, I would still be banging my head against the wall trying to figure it out if it wasn't for you. Also for discussion and inputs on this thesis.

I would like to thank **everyone else** who offered me their advice and who discussed this thesis with me. You know who you are.

A special thanks goes to my **fellow students** who dragged me away from my desk, making sure I got my breaks and keeping me sane.

Last of all, I thank my **family** and **friends** for motivation and support.

Contents

List of Figures

List of Tables

Abbreviations

AA	**A**rctic **A**mplification
AIV	**A**tmospheric **I**nternal **V**ariability
AO	**A**rctic **O**scillation
NAO	**N**orth **A**tlantic **O**scillation
PV	**P**otential **V**orticity
SST	**S**ea **S**urface **T**emperature
SWM	**S**tationary **W**ave **M**odel
THF	**T**urbulent **H**eat **F**lux

Chapter 1

Introduction

In the last century, global temperatures have risen, a phenomenon known as "global warming". The annual mean global mean surface temperature has been increasing since around 1900, with its largest trend at the beginning (0.098 °C/decade, average between the three datasets) and the end (0.156 °C/decade) of the century as seen in figure 1.1 from Hartmann et al. [13]. The main driver is the human induced increase of atmospheric greenhouse gas concentrations, along with the associated feedbacks.

The Arctic region has warmed more quickly than the rest of the globe during the global warming era and this warming has also accelerated in the last 15 to 20 years,

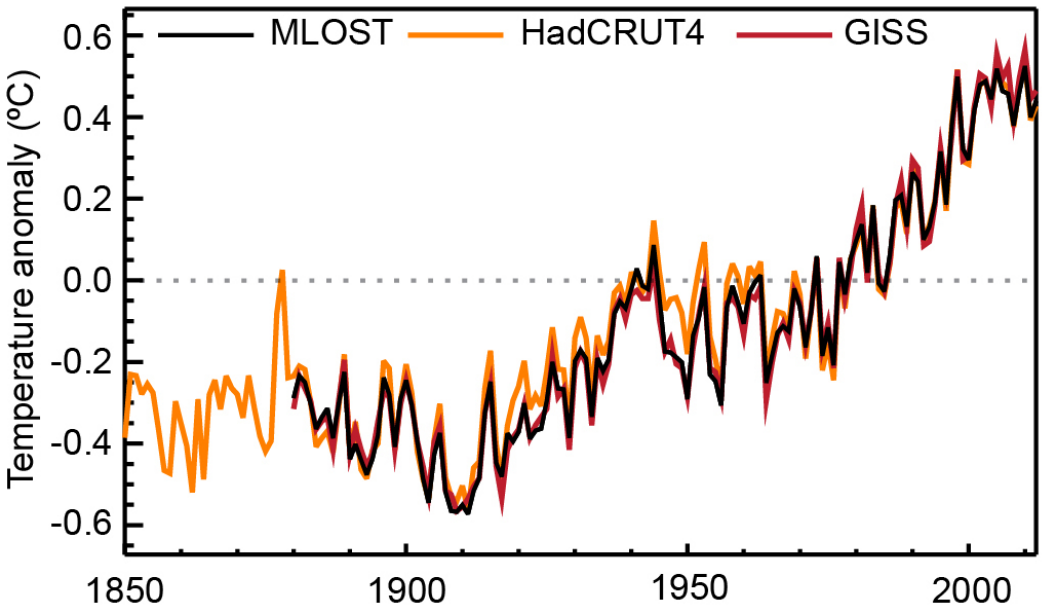

FIGURE 1.1: Annual global mean surface temperature anomalies relative to a 1961-1990 climatology from the latest version of the three combined land-surface air temperature and sea surface temperature (SST) data sets. (Hartmann et al. [13])

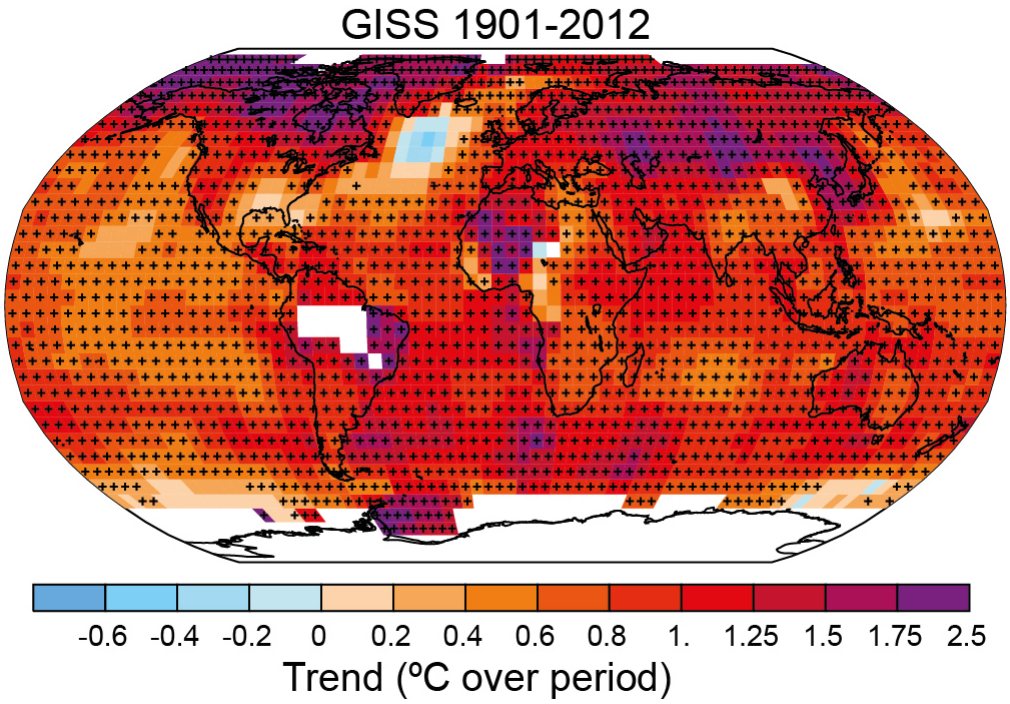

FIGURE 1.2: Trends in surface temperatures from the GISS data set of Figure 1.1 for 1901-2012. White areas indicate incomplete or missing data. Black plus signs indicate grid boxes where trends are significant at $p < 0.1$. (Hartmann et al. [13])

a phenomenon called Arctic amplification (AA). Several processes like sea ice retreat, snow-ice-albedo feedback, ocean heat transport and moist feedbacks contribute to AA, although there is debate about their relative importance (Alexander et al. [1], Brown et al. [3], Hall [12], Pithan and Mauritsen [26], Screen et al. [29], Taylor et al. [35]). The clearest signature of AA is the widespread enhanced temperature trend in the Arctic compared to the midlatitudes as seen in figure 1.2 from Hartmann et al. [13].

Along with global warming and AA, the northern hemisphere midlatitudes have experienced a number of extreme events in recent years which have caught the attention of both scientists and the public. These meteorological events occurred in a decade that was likely the warmest globally for a millennium (Coumou and Rahmstorf [8]). From a thermodynamic perspective, increased frequency of "warm" extreme events like heat waves or flooding is intuitively understood from a shift towards a warmer climate. Understanding the record breaking "cold" events that have occurred remains a scientific challenge (Wallace et al. [38]).

Francis and Vavrus ([10], [11]) hypothesize that AA lead to changes in the large-scale circulation and more frequent extreme weather of both warm and cold types in the midlatitudes. Their argument is that if the temperature warms more in the Arctic than elsewhere, this leads to a decrease in the midlatitude-to-pole geopotential thickness gradient. They describe two effects that could result from this. The first effect is that the

upper level westerly wind speeds decrease through the thermal wind relation, which in turn slows down Rossby wave propagation at upper levels. More slowly propagating Rossby waves are associated with more persistent weather conditions. A second effect of the geopotential thickness gradient decrease is that the Rossby waves tend to elongate meridionally and the jet stream becomes more wavy. This in turn affects surface conditions as cold polar air flows southward in the trough of the jet stream and warm equatorial air flows northward in the ridge of the jet stream. These two effects combined provide more persistent flow of polar or equatorial air into more southward or northward laying regions, thus enhancing poleward heat transport. Francis and Vavrus ([10], [11]) present results from analysis of NCEP/NCAR Reanalysis data which shows that the midlatitude-to-pole temperature and geopotential thickness gradients have decreased, zonal wind speeds have decreased, waves have extended meridionally, and the jet stream has become more wavy.

Other empirical and modeling studies examine a variety of mechanisms by which AA may change the atmospheric circulation. One mechanism is the sea ice forced pan-Arctic increase in geopotential height through anomalous ocean-to-atmosphere turbulent heat fluxes that shifts the phase of the North Atlantic Oscillation (NAO) or Arctic Oscillation (AO) (Alexander et al. [1], Honda et al. [16], Deser et al. [9], Cohen et al. [7]). The anomalous release of heat through sea ice decline has been shown to reduce the baroclinicity in the northern parts of the midlatitude storm tracks (Seierstad and Bader [32], Butler et al. [4], Jaiser et al. [19]) through a decrease in static stability near the surface. An equatorial shift of the jet stream has also been documented as a result of increased Arctic thermal forcing (Seierstad and Bader [32], Butler et al. [4]). The atmospheric circulation changes associated with AA have also been linked to to continental-scale wintertime cooling cooling (Outten and Esau [24]), either through anomalous cold air advection or increased moisture advection from the Arctic resulting in increased snow cover (Liu et al. [23], Cohen et al. [7], Honda et al. [16], Hopsch et al. [17]).

On the other hand, other studies find limited evidence for robust changes in the large-scale circulation during the AA period. Screen and Simmonds [31] find that the change in zonal and meridional Rossby wave amplitudes is limited to only a few seasons and wavenumbers in the ERA-Interim and NCEP/NCAR Reanalysis. They also argue that the atmospheric changes reported in Francis and Vavrus [10] are an artefact of the chosen methodology used in the analysis. Barnes [2] shows that the reduction of zonal wind speeds only affects the Rossby wave propagation during fall by using ERA-Interim, NCEP/NCAR Reanalysis and MERRA, concluding that the relation between the background flow and Rossby wave propagation is more complex than proposed in Francis and Vavrus [10]. Furthermore, Screen et al. [28] model the atmospheric response to

sea ice forcing and find that most of the sea ice signal is confined to low levels in the Arctic region. They also suggest that atmospheric internal variability (AIV) plays an important role in the midlatitude responses reported in many other studies.

The physical mechanisms whereby AA may be linked to anomalous midlatitude circulation are poorly understood from a dynamical perspective (Wallace et al. [38]). This study will deal with one of these proposed mechanisms: the direct impact of anomalous high latitude thermal forcing (where sea ice retreat and SST's play a central role, Screen and Simmonds [30]) on the midlatitude stationary waves. This study is distinguishable from other studies because it separates the effects of AA-related thermal forcing from other mechanisms which influence the circulation. Stationary waves provide a framework for understanding the large-scale circulation as they are closely related to the jet stream and storm tracks. The stationary waves relate to the Francis and Vavrus [10] because the changes in the Rossby waves they propose should alter stationary wave patterns and produce a wavier jet stream.

Chapter 2

Fundamentals of Rossby waves

The differential heating of the earth by the sun results in a warm equator and cool poles. The climate system must transport energy toward the poles to even out this imbalance. This creates midlatitude westerly jets in both hemispheres as the meridional flow is deflected by the Coriolis force, as well as other large-scale features of the atmospheric circulation such as the Hadley cells. There are continents and orography on earth which act as obstacles to the flow. These obstacles perturb the zonally symmetric flow, inducing waviness which forces the flow south (north) into wave troughs (ridges).

2.1 Free Rossby waves

The waves that come to exist by the wavy motion of the flow are called Rossby waves, which are governed by the dynamical constraints on large-scale atmospheric motions. In a baroclinic atmosphere, the wave is a potential vorticity (PV) conserving motion and therefore propagates on PV gradients. PV is determined by the relative vorticity induced by temperature differences, the large-scale latitudinal gradient in the Coriolis parameter, and the stratification of the atmosphere. It is a conserved quantity in a frictionless and adiabatic atmosphere. In a barotropic atmosphere, the Rossby wave is an absolute vorticity conserving motion. Absolute vorticity is the sum of the relative vorticity and the varying Coriolis parameter.

To explore the dynamics of the Rossby wave in a baroclinic atmosphere, we start from the shallow water PV equation (2.1)

$$PV = \frac{D}{Dt}(\frac{\zeta + f}{h}) = 0 \tag{2.1}$$

where ζ is the vertical component of the relative vorticity, f is the Coriolis parameter and h is the depth of the atmospheric layer.

Let's say a parcel moves from a deep layer to a more shallow layer. Since h reduces, so must ζ, f or both. At this point, only the relative vorticity can change since a change in f can only happen when the parcel moves meridionally. Assuming $\zeta = 0$ initially, after entering the shallow layer $\zeta < 0$, which is associated with anticyclonic vorticity. This means the parcel will start to move southward. With southward movement f will decrease, and at some point $\zeta + f = h$, but due to inertia in the system, the parcel will continue southward. After a further southward movement, $\zeta + f < h$ and the parcel will gain absolute vorticity, $\zeta > 0$ which will make the parcel move northhward. Again, this northward movement will increase f until $\zeta + f = h$ and so the oscillation continue. We see that this will make a trough-ridge pattern, with a trough where the atmospheric layer is shallower and a ridge where the atmospheric layer is deeper.

Now that we have established a general sense of how these waves work in terms of displacement and restoration, we expand the analysis by finding a dispersion relation for the wave. To simplify, we use (2.1) in a barotropic atmosphere ($h = const.$). Writing it out yields

$$\frac{D}{Dt}(\zeta + f) = 0 \tag{2.2}$$

$$\frac{\partial \zeta}{\partial t} + u\frac{\partial \zeta}{\partial x} + v\frac{\partial \zeta}{\partial y} + v\frac{\partial f}{\partial y} = 0 \tag{2.3}$$

$$(\frac{\partial}{\partial t} + u\frac{\partial}{\partial x} + v\frac{\partial}{\partial y})\zeta + v\beta = 0 \tag{2.4}$$

By using the perturbation method of Holton [15] (page 127-128) we linearize this equation about a zonal mean state, using

$$u = \bar{u} + u', v = v', \zeta = \frac{\partial v'}{\partial x} - \frac{\partial u'}{\partial y} = \zeta' \tag{2.5}$$

We define the streamfunction as

$$u' = -\frac{\partial \psi'}{\partial y}, v' = \frac{\partial \psi'}{\partial x}, \zeta' = \nabla^2 \psi' \tag{2.6}$$

This streamfunction is the inverse Laplacian of the relative vorticity. By a Fourier transform it can be shown that the streamfunction scales with the vorticity, but with opposite sign. This means that a positive value of the streamfunction is associated with negative (antcyclonic) vorticity, while negative values are associated with positive (cyclonic) vorticity. The first is equivalent to a geopotential ridge and the latter a geopotential trough, which is consistent with the streamfunction being the geopotential height scaled by f.

Combining (2.5) and (2.6), then inserting into (2.4) gives

$$(\frac{\partial}{\partial t} + \bar{u}\frac{\partial}{\partial x})\nabla^2\psi' + \frac{\partial \psi'}{\partial x}\beta = 0 \tag{2.7}$$

Assuming this equation describes a wave in the streamfunction, we seek solutions of the form

$$\psi' = Re[\psi_0 e^{i(kx+ly-wt)}] \tag{2.8}$$

where k and l are wavenumbers in the zonal and meridional direction, respectively, and w is the frequency. Solving (2.7) gives

$$c = \bar{u} - \frac{\beta}{k^2 + l^2} \tag{2.9}$$

where $c = w/k$ is the phase speed of the wave relative to the ground. We see that, relative to the mean wind, the Rossby waves always travel westward and that the speed is dependent on the length of the wave: short waves travel more slowly than long waves. On the other hand, the background zonal wind speed ($\bar{u}$) is generally larger than the phase speed, so that overall short waves propagate faster in the eastward direction than long waves.

2.2 Stationary waves

Certain types of Rossby waves exhibit stationary behavior when forced under special conditions, and these are termed stationary waves. The main forcings for the stationary waves in the Northern Hemisphere are orography and diabatic heating. These two forcings are not completely separable as orography contributes to determining the spatial pattern of diabatic heating and there are also other nonlinear interactions between these forcings (Ringler and Cook [27]).

Starting with (2.9) and setting $c = 0$ for a wave with zero phase speed relative to the ground, we get

$$k^2 + l^2 = \frac{\beta}{\bar{u}} = K_s^2 \tag{2.10}$$

We see that the wave becomes stationary at certain wavenumbers, dependent on the zonal wind speed. K_s^2 is hereafter called the stationary wavenumber.

To investigate the properties of forced stationary waves, we introduce a simple forcing in equation (2.7)

$$(\frac{\partial}{\partial t} + \bar{u}\frac{\partial}{\partial x})\nabla^2\psi' + \frac{\partial \psi'}{\partial x}\beta = -f_0\bar{u}\frac{\partial D}{\partial x} \tag{2.11}$$

where D is diabatic heating and $f_0 = f - \beta$, a reference Coriolis parameter. Assuming wavelike solutions for this forcing, we can solve this equation by using a steady state version ($w = 0$) of (2.8) and

$$D = Re[D_o e^{i(kx+ly)}] \tag{2.12}$$

This gives the result

$$\psi_0 = \frac{f_0 D_0 \bar{u}}{\bar{u}(k^2 + l^2) - \beta} \tag{2.13}$$

which can be rewritten (using $k^2 + l^2 = K^2$)

$$\psi_0 = \frac{f_0 D_0}{K^2 - K_s^2} \tag{2.14}$$

From this we see that forced Rossby waves can become quasi-resonant when the wavenumber gets close to the stationary wavenumber (friction, which we ignored, ensures that they never become completely resonant in the real world). The quasi-resonance is responsible for the stationary waves becoming amplified, it causes pronounced ridges and troughs which create the characteristic climatological ridge-trough pattern. This has implications for the jet because the jet's position is partially determined by the stationary waves. It also has implications for midlatitude weather as the stationary waves also act as waveguides for synoptic-scale waves.

The stationary waves are persistent features of the large-scale circulation due to the anchoring effect of the dominant forcing mechanisms. Figure 2.1 shows the January mean

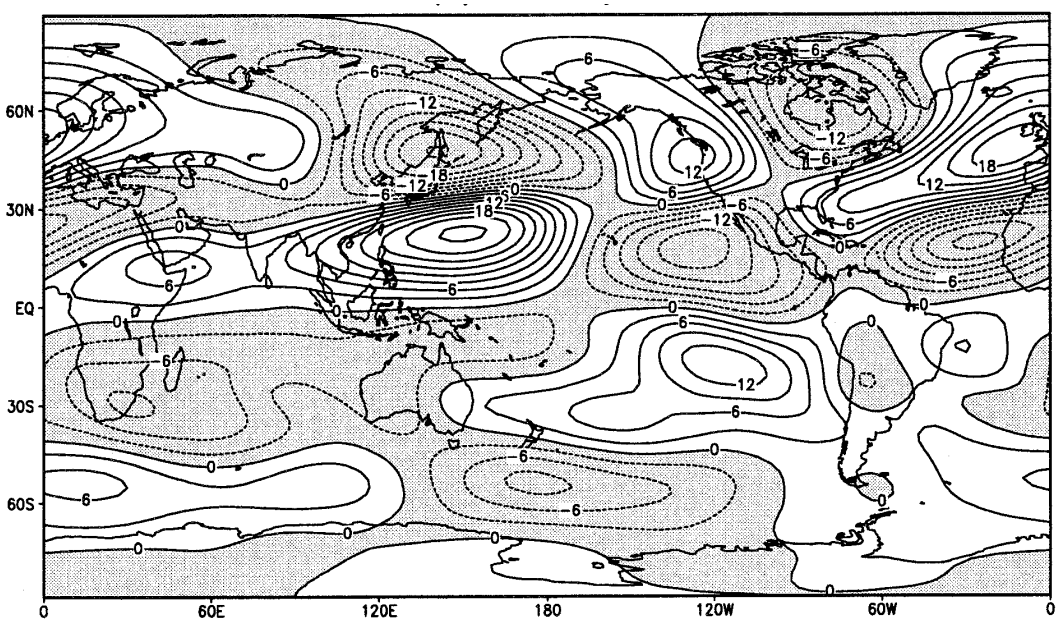

FIGURE 2.1: January streamfunction at $\sigma = 0.257$ from NCEP-NCAR Reanalysis. Solid contours are positive values whiles dotted and shaded contours are negative values. Contour interval is $3 \cdot 10^6 m^2/s$ (from Held et al. [14])

upper level streamfunction. The first thing to notice is the hemispheric differences. The reason for this difference is the fraction of continents in the hemispheres. The Northern Hemisphere is more land covered which gives exchanges in diabatic heating through land-sea thermal contrasts and there is more orography, specifically large mountain ranges here. This makes it more likely to create stationary waves as we see. We see in the streamfunction field characteristic ridges and troughs associated with interaction with topography and heating at the coastal boundaries of the Pacific- and the Atlantic Oceans.

Chapter 3

Arctic climate change

3.1 The Arctic amplification period

In the last decade a clear weakening of the near-surface equator to pole temperature gradient has emerged (Cohen et al. [6], Screen and Simmonds [30]), though causal mechanisms have been (and to some extent still are) debated. The decrease in the lower tropospheric temperature gradient is one of the most clear signs we have of AA. The weaker gradient is seasonally robust and strongest in fall and winter (Cohen et al. [6], Screen and Simmonds [30]). Initially, it was thought to be caused solely by sea ice decline and related surface albedo feedbacks since the largest decline in sea ice extent and temperature amplification began at approximately the same time in the 2000s. Modeling studies confirm that these processes are important contributors to the Arctic surface warming (Taylor et al. [35], Screen et al. [29]), but AA can also occur without a reduction in the surface albedo (Hall [12]) or sea ice (Pithan and Mauritsen [26]) because low level clouds, moisture, lapse rate and greenhouse gas feedbacks also affect AA. Through an increase in equator-to-pole atmospheric heat transport, the middle and upper parts of the Arctic atmosphere are also warming more than the global mean, but not nearly as much as near the surface (Screen et al. [29]).

Henceforth, the AA period is defined as 2001-2013 and the climatological period as 1981-2000, so that anomalies are anomalies of the AA period with respect to climatology.

The temperature anomalies during the AA period in the Arctic vary geographically and over the seasonal cycle, as is the case for sea ice anomalies. Generally, the warm temperature anomalies appear where ice starts to form in autumn as a response to the ocean giving up heat to the atmosphere. Indeed, this happens every year, but the anomalously low ice during the AA period in certain regions compared to climatology

gives pronounced temperature anomalies in these regions. In September, the sea ice is at minimum and there are widespread positive temperature anomalies, with the largest anomalies in the Chukchi Sea (figure 3.1 (a)). During September the Arctic Ocean is able to store more of the radiation as heat because of the extra bare ocean compared to other months which can be released to the atmosphere. During October, sea ice starts to form in the Chukchi Sea and East Siberian Sea, releasing large amounts of the heat stored in the ocean to the atmosphere. In these regions, the temperature anomaly spreads out and amplifies in magnitude (figure 3.1 (b)). By the end of the month, these regions are fully covered in ice. A positive temperature anomaly, almost as strong as the Chukchi one appears in the Barents and Kara Sea. By November, the Chukchi temperature anomaly weakens but its placement is almost the same as in October, while there is not much change to the Barents/Kara temperature anomaly (figure 3.1 (c)). A small anomaly in the Baffin Bay appears. In December, the Chukchi anomaly further weakens and contracts (figure 3.1 (d)), which is not surprising as this region has been fully covered in ice since November. On the other hand, the Barents/Kara anomaly intensifies and expands in this month probably due to the fact that the ocean to atmosphere heat fluxes are large as there is anomalously low ice cover. In January and February (figure 3.1 (e) and (f)) the temperature anomalies contract in extent. They weaken slightly in the Barents/Kara Seas and intensify over Baffin Bay.

We have looked at the general characteristics of temperature anomalies during the AA period, but there is considerable interannual variability. One example is the all time record minimum of sea ice that happened in mid-September 2012. The temperature anomalies mainly followed the spatial pattern from figure 3.1, but the magnitude of the anomalies were up to twice as large. The special case of 2012 was caused by both special preconditioning of the system during the previous (2011/2012) season and two intense storms during late summer in 2012 (Parkinson and Comiso [25], Simmonds and Rudeva [33]). During the freeze up season after the 2011 melt, the ice cover was almost back to the mean 1990s extent. In contrast to the mean 1990s sea ice, much of the ice formed in 2011/2012 was first year ice whereas a large fraction of the 1990s consisted of multiyear ice, which is thicker and thereby more persistent to melting. By summer 2012, most of the new ice had melted away largely because of warmer SSTs melting the ice from underneath. By the end of the summer, the sea ice extent was even lower than it was at the same time in 2007 (previous record minimum). Shortly after, in late August, a very intense cyclone appeared from Siberia and traveled across the Arctic Ocean, dissipating in the Canadian Archipelago. In the meantime, another cyclone appeared over northern North America and traveled towards Siberia. Both of these cyclones led to large portions of ice being ripped away from the main ice pack and transported away

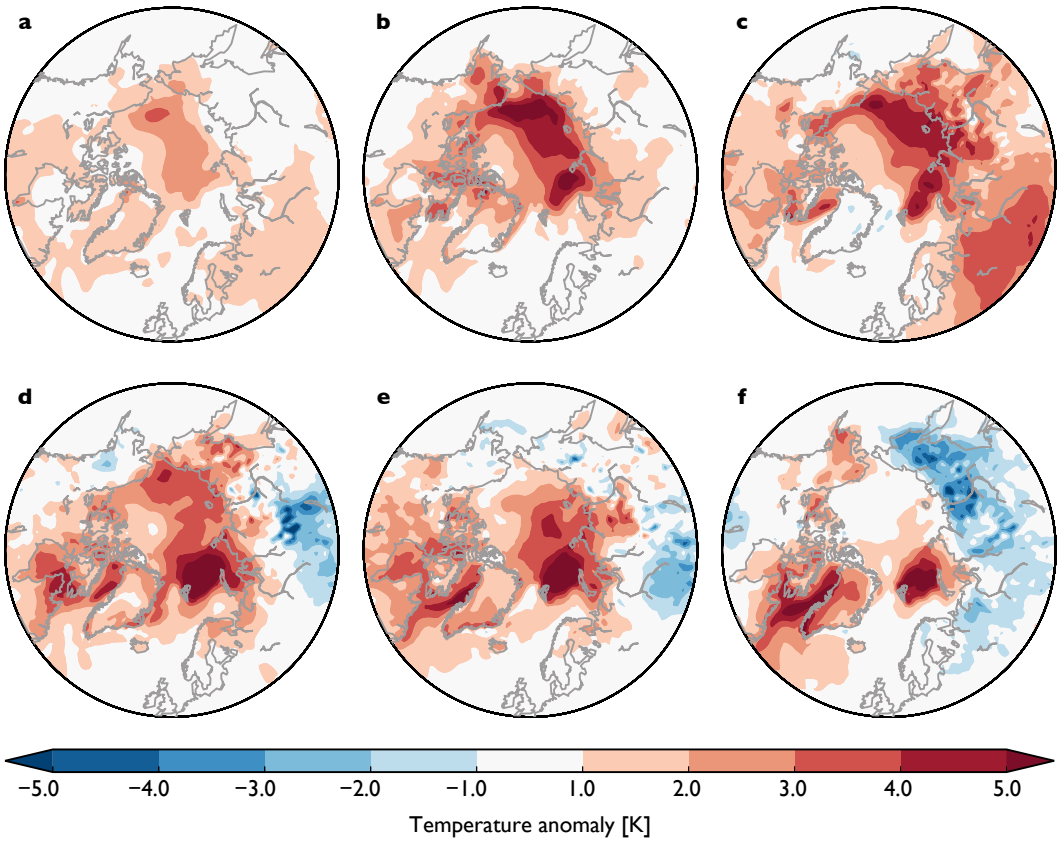

FIGURE 3.1: Anomalies of 2m temperature [K] in the AA period compared to climatology for (a) September, (b) October, (c) November, (d) December, (e) January and (f) February. Data from ERA-Interim reanalysis.

and melted, contributing to the lowest sea ice extent on record. As we see, there are factors other than the "classical" AA processes that can lead to a low sea ice year.

Certain aspects of the observed changes in the Arctic atmosphere and cryosphere are associated with changes in diabatic heating (figure 3.2). For the discussion to follow, we focus on wintertime as it is the season where the Arctic climate has experienced large changes during the AA period and it is the season where reportedly AA has most influence on the remote atmospheric circulation. In figure 3.2 (a) we see the sea ice extent shows a significant decrease in the AA period compared to climatology. As mentioned, this decline in sea ice extent is a large contributor to AA. By having reduced sea ice extent during winter, the time when the ocean is able to provide heat to the atmosphere through turbulent heat fluxes (THFs) is prolonged and the area where this can happen extended. The albedo in figure 3.2 (b) shows a negative trend although the decrease during the AA period is only significant at the 95% level. Since there is little land above 65°N, this albedo decrease is mostly related to decrease in sea ice and on-ice snow cover. During winter, much of the newly formed ice is thin and fractured and not effective at insulating the atmosphere from the ocean. However, snow on top of ice is very effective at insulating atmosphere from ocean. A reduction of snow cover (Brown et al. [3]) at high

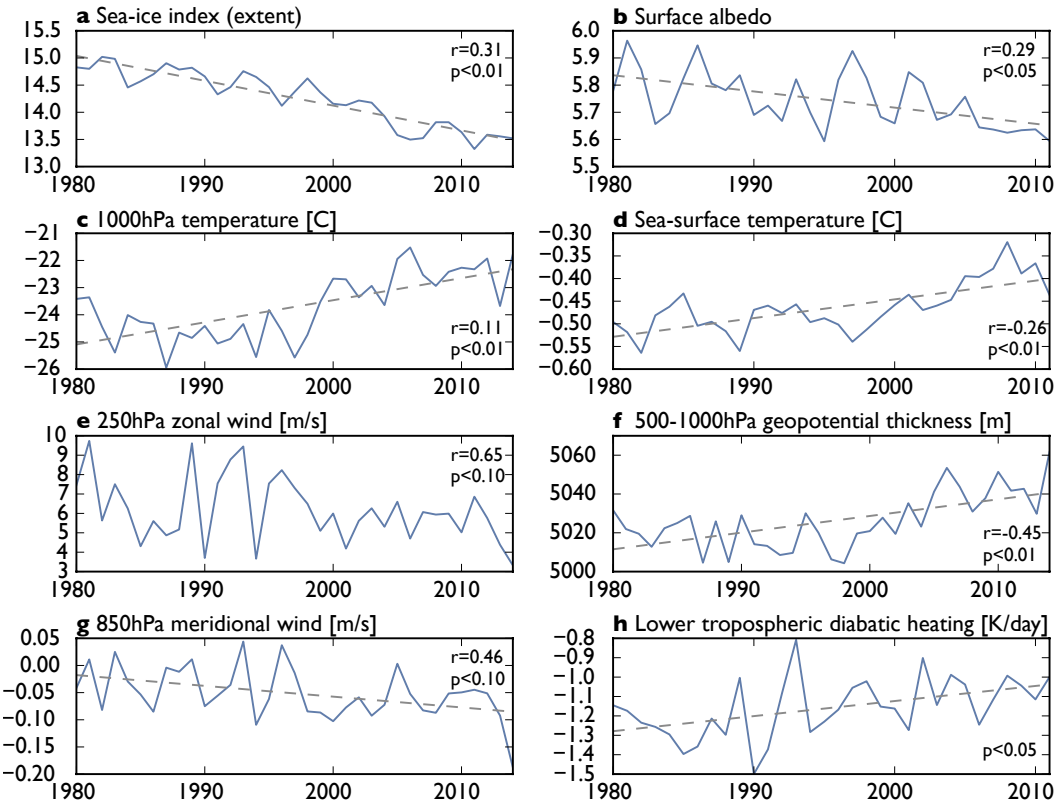

FIGURE 3.2: Winter (DJF) season time series area-averaged over the Arctic (65°N-90°N: (a) sea ice extent, (b) surface albedo, (c) 1000hPa temperature [°C], (d) Sea surface temperature [°C], (e) 250 hPa zonal wind [m/s], (f) 500-1000hPa geopotential thickness [m], (g) 850hPa meridional wind [m/s], (h) Mass weighted average (925-700hPa) of diabatic heating [K/day]. Indicated at the top right of each panel are the correlation coefficient (r) with the diabatic heating time series (panel h) and the statistical significance (p) of the shift in the median during the AA period using a Wilcoxon ranksum test. Time series with statistically significant linear trends are marked by a dashed grey line showing the linear trend. Data from (a) NSIDC, (b) NOAA-CIRES 20th Century Reanalysis, (c) NCEP/NCAR Reanalysis, (d) COBE-SST2, (e)-(h) NCEP/NCAR Reanalysis.

latitudes could thus increase ocean to atmosphere THFs. Also, since bare ice has lower reflectivity than snow covered ice, less snow increases the direct radiative warming. We see that Arctic mean temperature (figure 3.2 (c)) has had a significant increase during the AA period. A significant increase in SST's (figure 3.2 (d)) are also found for the Arctic domain during the AA period. The cause of the increase is probably the ocean being able to store more heat during the year as ice cover has decreased. Another cause that might be contributing is increased ocean heat transport from midlatitudes as the oceans here are anomalously warming in response to global warming (Pithan and Mauritsen [26]). The increased SST's increase the ocean to atmosphere heat fluxes. The 250hPa zonal winds have not changed significantly during the AA period (figure 3.2 (e)). Zonal wind speeds are seemingly decreasing, which could lead to more slowly propagating Rossby waves in the Arctic. However, as pointed out in the introduction, this is not a one-to-one relationship. The 500-1000hPa geopotential thickness in figure 3.2 (f) shows

a significant increase, and is highly correlated (r=0.87) to the temperature. As with the 250hPa zonal winds, the 850hPa meridional winds have not changed significantly either, although they exhibit a decreasing linear trend meaning a more southward flow (figure 3.2 (g)). A possible effect of this is enhanced advection of polar air into lower laying regions. Lower tropospheric (925hPa-700hPa) diabatic heating as seen in figure 3.2 (h) also exhibits a positive trend although the increase during AA is not significant.

The correlation coefficient indicated in each figure shows the correlation of that time series to the lower tropospheric diabatic heating (figure 3.2 (h)). We see some obvious relationships in the correlations, for example increased temperatures, SSTs and decreased sea ice extent with increased diabatic heating, although the correlations are not strong. This reflects on the complexity of relating diabatic heating to different processes.

3.2 Arctic diabatic heating

"[Diabatic] heating provides the sources and sinks of heat which drive the global circulation" (James [20], page 73). The climate system is heated by short wave solar radiation. With diabatic heating generated, several exchanges of heat take place which act to redistribute the atmospheric pattern of diabatic heating. There are several ways heat is exchanged, for example through surface exchanges, changes in the phase of fluids in the atmosphere or advection. It is the distribution of the diabatic heating which drive the global circulation, and this circulation again act to redistribute diabatic heating. Diabatic heating can be lost from the atmosphere through long wave outgoing radiation to space.

The exchanges of diabatic heat vital for the atmospheric circulation are hard and expensive to measure explicitly. Instead, methods to diagnose the net diabatic heating from reanalysis have been used, and in this study we use the "residual method" (Chan and Nigam [5]). By this method, the diabatic heating is calculated as a residual of the thermodynamic equation which provides a reasonably accurate measure of the net heating of the atmosphere. However, this method does not distinguish between the contributions of all the relevant processes to the heat exchange. Heating was only calculated from NCEP/NCAR Reanalysis and it is important to note that there are differences between reanalysis products (Chan and Nigam [5], Ling and Zhang [22]) using this method.

The seasonal cycle of diabatic heating anomalies during the AA period varies geographically and in intensity. The diabatic heating anomalies have a more noisy spatial distribution than the temperature anomalies, especially on a monthly scale. The field smooths

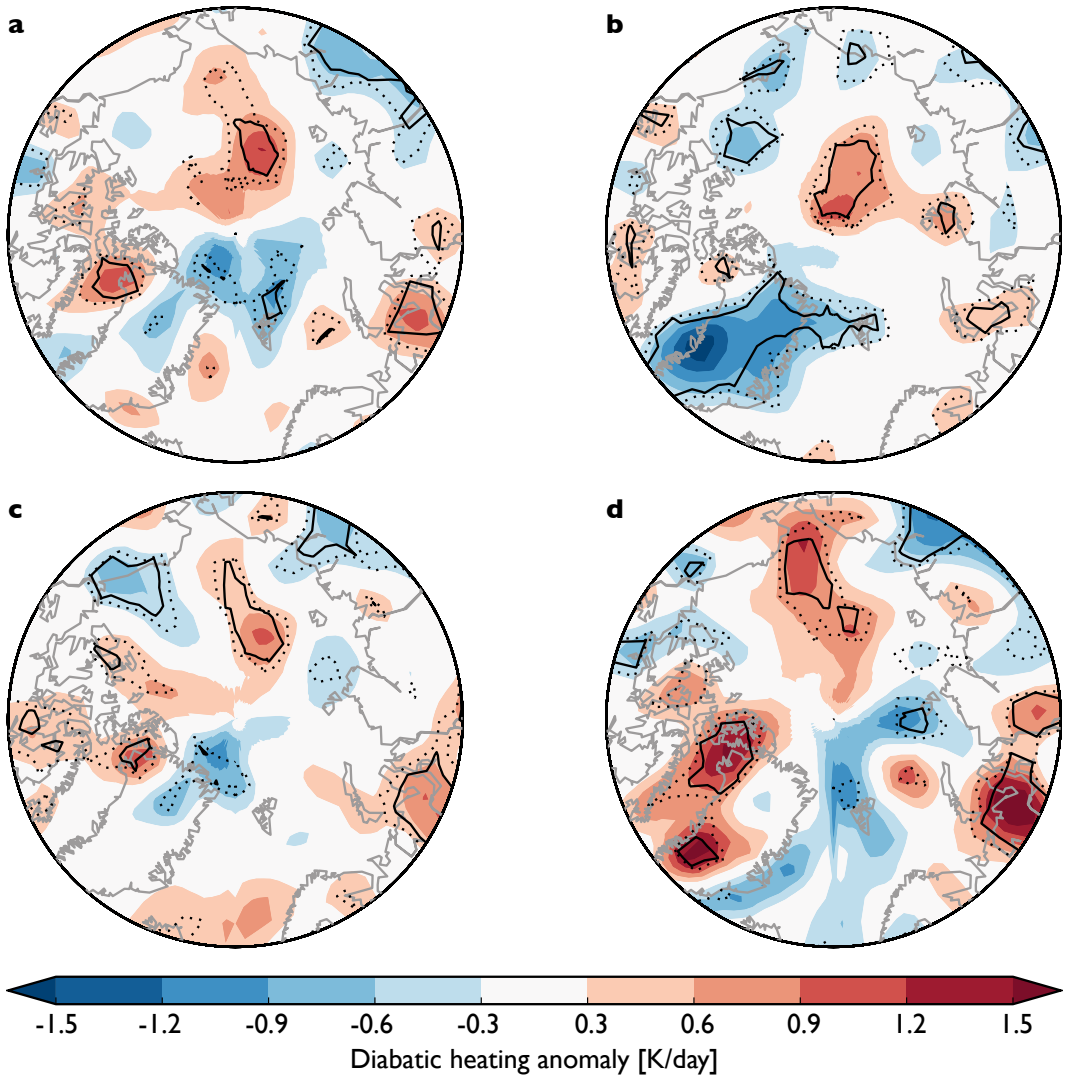

FIGURE 3.3: Seasonal anomalies of diabatic heating [K/day] in the AA period in the lower troposphere (mass-weighted average from 925-700hPa) for (a) MAM spring, (b) JJA summer, (c) SON fall and (d) DJF winter. Black lines show regions where the anomalies are significant at a level of p=0.05 (dashed) and p=0.01 (solid) according to a Wilcoxon ranksum test. Derived from NCEP/NCAR Reanalysis.

somewhat when using seasonal averages and therefore we present the seasonal distribution of Arctic diabatic heating anomalies rather than monthly. Statistical significance of the diabatic heating anomalies is limited, unsurprisingly, as the AA period is short. During spring the heating anomalies are located mainly in the central parts of the Arctic ocean, Baffin Bay and near the Kara Sea (figure 3.3 (a)). However, the zonal mean structure of anomalies shows no significant increase (or decrease) of diabatic heating in the AA period (figure 3.4 (a)). In summer, the central parts of the Arctic ocean show positive heating while a large and intense (down to -1.5K/day) cooling anomaly sets over Greenland (figure 3.3 (b)). In the zonal mean vertical structure, cooling of the Arctic at 70°N is significant from the lower troposphere up to 550hPa (figure 3.4 (b)). In fall (figure 3.3 (c)) we see that the anomalous heating in the central Arctic persists

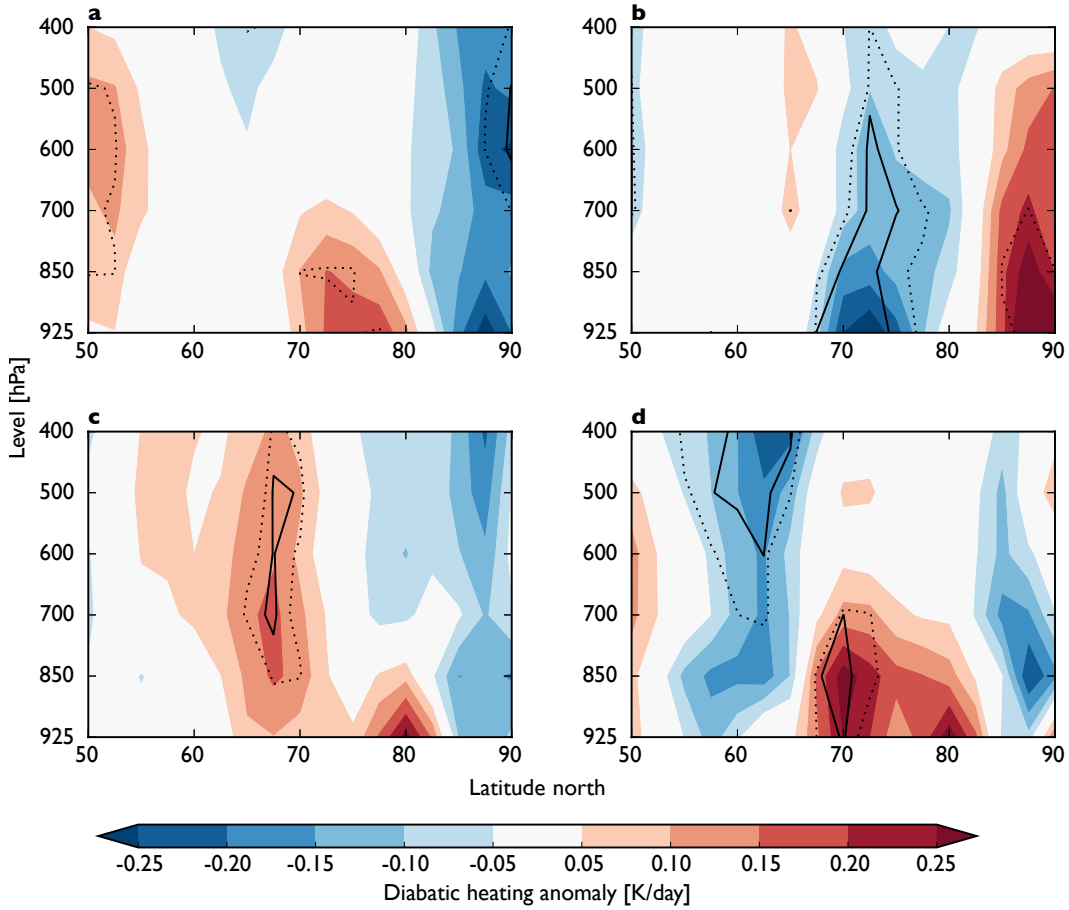

FIGURE 3.4: Seasonal anomalies of diabatic heating [K/day] in the AA period, zonally averaged, for (a) MAM spring, (b) MAM spring, (c) JJA summer and (d) DJF winter. Black lines show regions where the anomalies are significant at a level of p=0.05 (dashed) and p=0.01 (solid) according to a Wilcoxon ranksum test. Derived from NCEP/NCAR Reanalysis.

and a heating anomaly appears in Baffin Bay and a cooling anomaly appears in the Beaufort Sea. There is very little significance in the zonal mean vertical structure of the anomalies during this season (figure 3.4 (c)). In winter, heating anomalies appear in the southwestern Greenland and Barents-Kara Seas (figure 3.3 (d)). The central heating anomaly expands and its strongest heating shifts toward the Chukchi Sea. The Baffin Bay heating anomaly expands and intensifies. The heating anomalies peaks in intensity during this season, showing anomalous heating of up to 1.5 K/day. In the zonal mean, only lower tropospheric heating is significant at 70°N (figure 3.4 (d)). For all seasons it is difficult to point to causes and determine the relative contribution of different processes for anomalous heating or cooling.

As mentioned, using the residual method to diagnose diabatic heating leaves us unable to identify the contribution of different processes involved in creating the observed diabatic heating anomalies. The use of statistical methods still does not let us identify processes for exchanges, but could give us clues. Here we try to correlate the wintertime heating to

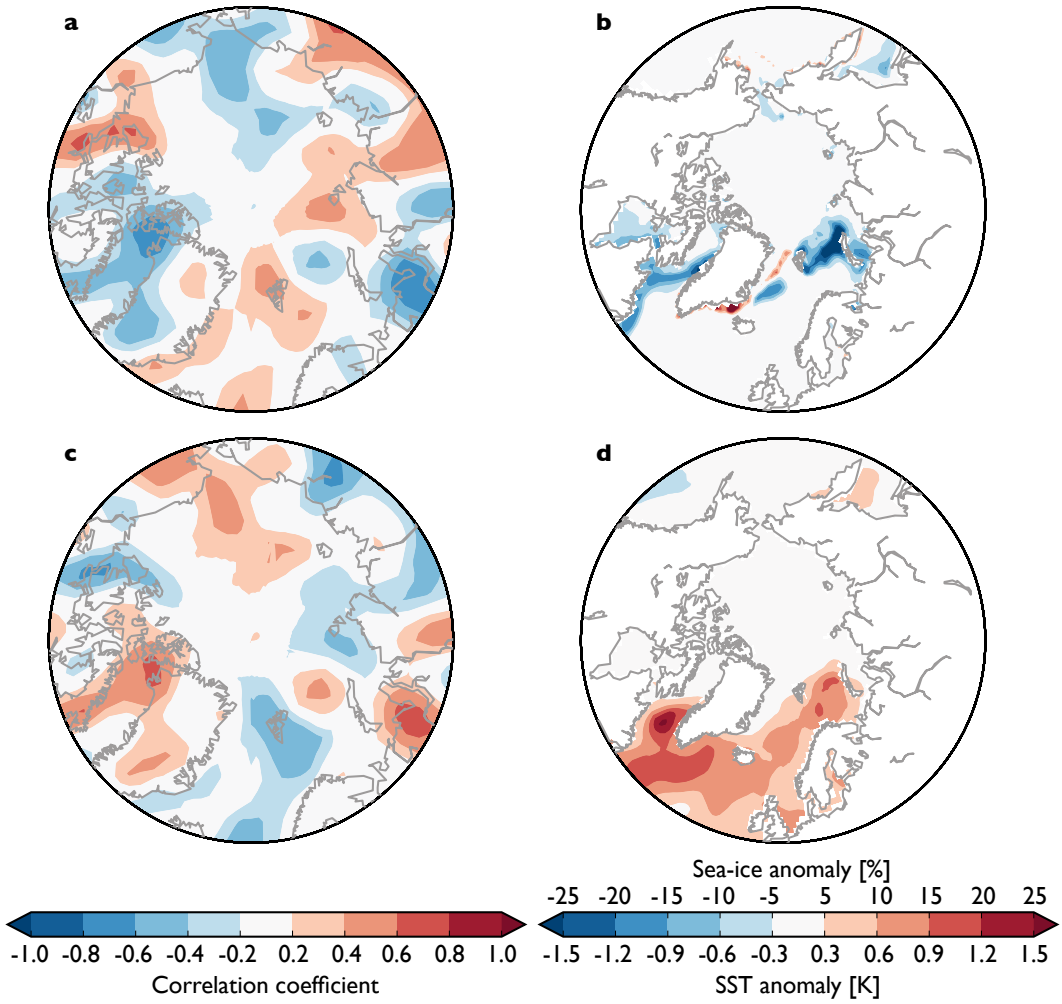

FIGURE 3.5: Relationships between diabatic heating, sea ice concentration and sea surface temperature for DJF winter. (a) One-point correlation coefficient map between area averaged (65°N-90°N) sea ice concentration and diabatic heating in the lower troposphere (mass-weighted averages from 925 to 700hPa), (b) anomalies of sea ice concentration [%] in the AA period, (c) One-point correlation coefficient map between area averaged (65°N-90°N) sea surface temperature and diabatic heating in the lower troposphere (mass-weighted averages from 925 to 700hPa), (d) anomalies of SST [K] in the AA period.

the sea ice index and SSTs (figure 3.5 (a) and (c)). The time series from figure 3.2 (a) and (d) are correlated grid point by grid point to the mass-weighted column-averaged lower tropospheric diabatic heating field. Figure 3.5 (a) shows anomalous heating associated with sea ice decline in Baffin Bay, Kara Sea and Chukchi Sea. The same regions appear to be associated with heating when correlated with SST's in panel (c). However, it is only in Baffin Bay and Kara Sea where the anomalous heating is collocated with the sea ice and SST anomalies (figure 3.5 (b) and (d)) and therefore the regions where we might expect to find a direct link.

Chapter 4

Stationary wave model

To investigate the mechanisms through which AA-related diabatic heating might influence the midlatitude atmospheric circulation, a simplified approach is warranted. To this end, a linear stationary wave model (SWM) is employed for computing global stationary wave patterns. The model has been shown to reproduce the observed stationary waves well in several studies (Held et al. [14], Sobolowski et al. [34], Ting [36], Ting [37], Wang and Ting [39]). Due to the linearity of the model, determining the contribution from different forcing mechanisms is done simply by exclusion/inclusion. This provides an ideal simplified framework for identifying the direct response of the atmospheric circulation to AA-related forcings.

The model is driven by a zonal mean basic state as well as zonally asymmetric forcings. The required inputs may be computed from GCM or reanalysis data. The forcings are the following: basic state (zonal wind, meridional wind, temperature, surface pressure and sigma dot vertical velocity), diabatic heating, orography, transient forcing and stationary nonlinearty (tendency in temperature, surface pressure, divergence and vorticity). The basic state provides the zonal mean state which the model is linearized about. Diabatic heating is calculated as in chapter 3 and includes the transient heat flux. The transient forcing component accounts for the eddy momentum fluxes. Orographic forcing represents the stationary wave forcing by mountains and terrain. This linear model does not allow for interaction between waves forced by the different forcing terms or wave-mean flow interaction, which are important contributors to the climatological waves. For this reason, the stationary nonlinear forcing term is added to account for these interactions. For all the forcing components, it is only the zonally asymmetric components that contribute to the stationary wave response.

The model runs for a year with monthly steady-state solutions for each experiment. First, it linearizes about the zonal mean flow. It then divides the zonally asymmetric

part of the basic state into wavenumbers and sets up a matrix (A) with these. Next, the model divides the forcing terms into wavenumbers and puts these in another matrix (B). The matrix equation then is $AX = B$ and X, the response, is found by matrix inversion.

Some technical details about the model follows. The model uses an R30 (rhombial wavenumber 30 truncation) grid which is approximately 2.25° latitude × 3.75° longitude in the horizontal. In the vertical, the model has 14 unevenly spaced sigma levels. It is a baroclinic model and has mass conservation and hydrostatic equations included. Damping in the form of Raylaeigh friction and Newtonian cooling is present at the lowest levels to represent momentum and heat transfer with the surface, and also biharmonic diffusion is included to remove small scale noise at all levels.

4.1 Control run (CTRL)

For the control run, daily NCEP/NCAR Reanalysis data for the period 1981-2000 were obtained (Kalnay et al. [21]). The data downloaded were zonal wind (u), meridional wind (v), temperature (T), surface pressure (ps) and surface geopotential height (hgt). The daily fields were then averaged into monthly means over all years to produce the climatological data.

Next, we calculated the climatological forcing inputs for the SWM. The data described in the previous paragraph were first interpolated to the R30 grid and then interpolated onto sigma surfaces. This gave the basic state (except for vertical velocity which was calculated after interpolation) and orography. The nonlinear forcing term was then calculated from the climatological data on the model grid. The transient forcing was calculated by using equation (2) from Wang and Ting [39] . Diabatic heating was pre-calculated according to Chan and Nigam [5] and interpolated onto the model grid.

The control simulation was able to reproduce the observed stationary waves from re-analysis (comparing figure 2.1 and 5.1 (a))

4.2 Experimens

4.2.1 Arctic amplification related diabatic heating (AADIA)

The first experiment was set up to test if Arctic amplification related anomalous diabatic heating could drive a direct midlatitude stationary wave response. Idealized heating

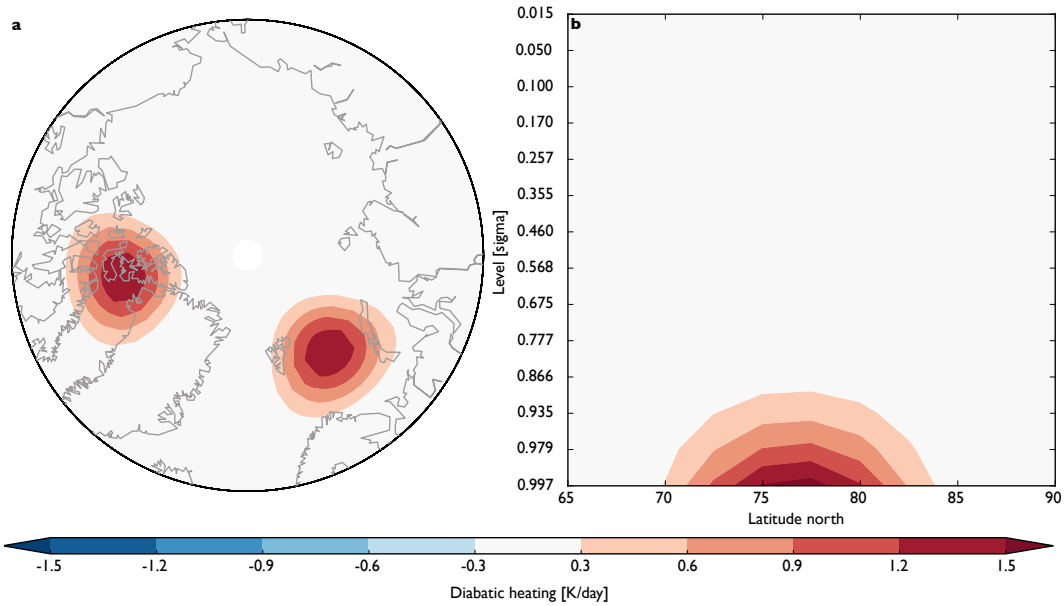

FIGURE 4.1: Imposed diabatic heating anomalies [K/day]. (a) synoptic map of the $\sigma = 0.997$ surface. (b) Zonal mean of the Baffin Bay anomaly. For (b) the colors were scaled with a factor of 0.25 to the colorbar.

anomalies to represent surface related AA processes were created, as seen in figure 4.1 (see appendix A for a detailed description of these heating anomalies). These anomalies are based on the wintertime AA anomalous diabatic heating from figure 3.3 (d). The reason for this choice is that these were the anomalies that are probably most closely related to the AA surface processes (sea ice decline and warming SSTs). For simplicity, these two anomalies have the same extent (80° longitude x 17° latitude), magnitude (maximum 1.5K/day) and depth (from surface to σ=0.866). Extent, magnitude and depth are realistic compared to reanalysis.

These anomalies were superimposed on the diabatic heating field from CTRL and kept the same for every month in this experiment. The basic state and other forcings were the same as in CTRL.

4.2.2 Temperature gradient reduction (TGR)

This experiment looks at whether the overall Arctic warming which decreases the equator-to-pole temperature gradient, is a mechanism contributing to changes in the midlatitude circulation, as proposed by Francis and Vavrus [10]. Here a composite of the 2001-2013 temperature anomalies (figure 3.1) were added to the CTRL basic state between 70°N - 90°N and 1000hPa-700hPa. Stationary nonlinear forcing was recalculated with respect to this basic state temperature change. The diabatic heating forcing term includes the

transient heat flux and therefore we imposed the AADIA heating perturbation. The other forcing terms were kept to CTRL.

4.2.3 Varying Arctic basic state (ARC)

The next set of experiments were done to address the question of whether or not the change in the wintertime basic state during the AA period provides a preconditioning which promotes a midlatitude stationary wave response. In contrast to TGR, this included adding the anomalies for ps, u and v as well as T. The basic state was varied from 65°N - 90°N (anomalous pressure patterns probably related to AA are evident slightly further south than the temperature amplification) and between 1000hPa-700hPa using monthly 2001-2014 fields from reanalysis, while the rest of the basic state was kept to CTRL. Instead of adding anomaly composite of 2001-2014, anomalies from individual years were added. The heating forcing from AADIA was used and the rest of the forcings were the same as the CTRL.

4.2.4 Varying global basic state (GLO)

The last set of experiments takes into account midlatitude atmospheric variability and possible preconditioning for the stationary wave response on the global scale. Here 2001-2014 anomalies were added to the CTRL basic state as in ARC, but globally instead of limited to the Arctic. The heating forcing from AADIA was used and the rest of the forcings were the same as the CTRL.

4.2.5 Sensitivity study

A sensitivity study of the stationary wave response to AA related anomalous diabatic heating was also carried out. This can be found in Appendix A.

4.3 Summary of experiments

Experiment	Basic state Arctic	Global	Diabatic heating	Nonlinear forcing	Transient forcing + orography
CTRL	Climatology	Climatology	Climatology	Climatology	Climatology
AADIA	Climatology	Climatology	Climatology + anomaly	Climatology	Climatology
TGR	2001-2013 composite	Climatology	Climatology + anomaly	Climatology + 2001-2013 composite (Arctic)	Climatology
ARC	2001-2014	Climatology	Climatology + anomaly	Climatology	Climatology
GLO	2001-2014	2001-2014	Climatology + anomaly	Climatology	Climatology

Chapter 5

Results

We now turn to the results of the experiments described in chapter 4. Only the wintertime responses are shown as the forcing was based on the wintertime heating and the seasonal response to the same forcing is highly invariable (not shown). In the following, "response" refers to the difference between the model run of a particular perturbation experiment and the CTRL.

5.1 AADIA

The direct stationary wave response to realistic diabatic heating anomalies is relatively strong in the Arctic, while no midlatitude response is evident (figure 5.1 (a)). The response has a baroclinic structure and the response weakens with height from surface up to $\sigma = 0.866$ whereafter the response increases in strength with height. In the upper levels a ridge over Baffin Bay appears above the Baffin Bay heating anomaly. It extends into the Barents Sea where Barents/Kara anomaly was placed, but is weaker in this region. This response is collocated with the climatological stationary trough over the Baffin Bay and Canadian Archipelago and indicates a weakening of the climatological pattern. The result of this is a southward contraction of the trough from climatology, implying changes in upper level southward polar air transport into this region. On the European side the ridge response is weaker, but it does somewhat amplify the climatological stationary ridge here and extend it in the zonal direction towards Greenland. The cyclonic response centered over the East Siberian Sea suggests a poleward extension of the the west Pacific cyclone from climatology. In contrast to the Canadian Archipelago response, this could provide a pathway for anomalous upper level poleward flow into the East Siberian Sea.

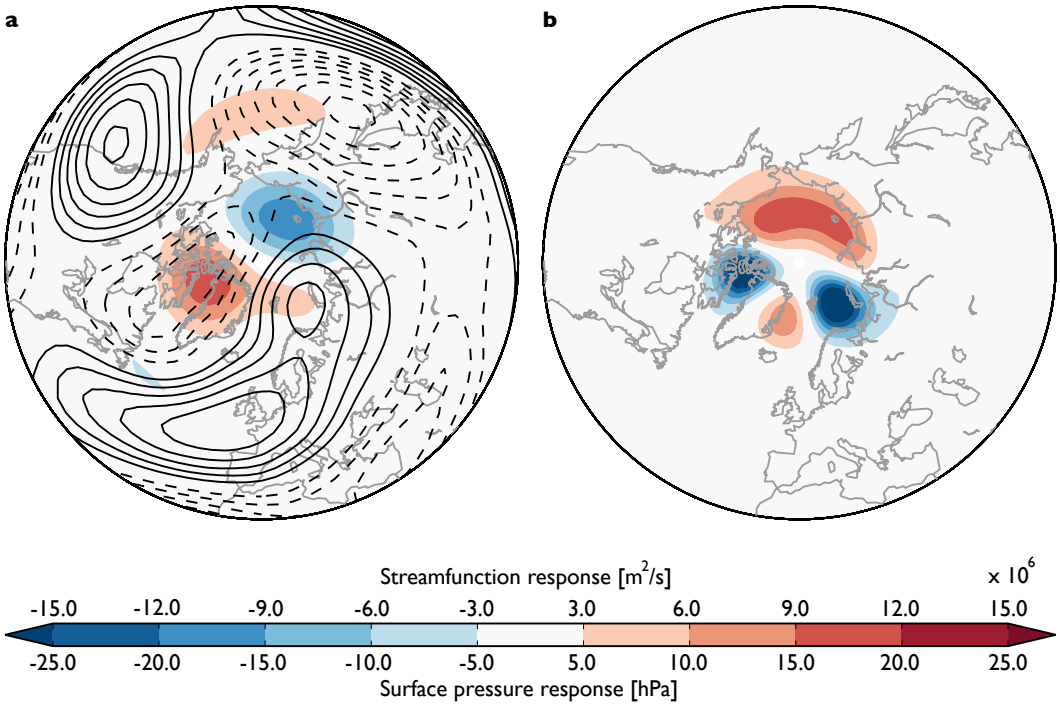

FIGURE 5.1: (a) Streamfunction response in colors and streamfunction from control in contours (negative values dashed), both at $\sigma = 0.257$. Contour interval as the colorbar. (b) Surface pressure response

As with the stationary waves, the surface pressure response is also confined to the Arctic (figure 5.1 (b)). We see two cyclonic surface pressure centers in response to anomalous heating where heating was imposed. This is expected as heating results in upward vertical motion and therefore a vertical divergence of mass near the surface. There is also two high pressure centers between the low pressure centers, which is dynamically consistent. These surface pressure responses are situated too far north to project onto the NAO, an argument strengthened by the fact that the response is not barotropic.

Apart from a slight weakening of the zonal winds in the Pacific jet exit region, the jet stream is largely unaffected by the AADIA forcing (figure 5.2 (a)). The most prominent upper level zonal wind response is a reduction of the zonal wind speed over Baffin Island and increase in zonal wind speed near the Bering Strait. Due to the baroclinic nature of the response this would lead to an increase (decrease) of the vertical wind shear, which could lead to an increase (decrease) of baroclinicity on the poleward flank of the North Pacific (North Atlantic) storm tracks.

Lower level meridional wind responses are also confined to the Arctic (figure 5.2 (b)). We see that the meridional wind response strengthen the climatological patterns, with southward flow over the Barents Sea and Canadian Archipelago and northward flow over East Siberian Sea and over Greenland.

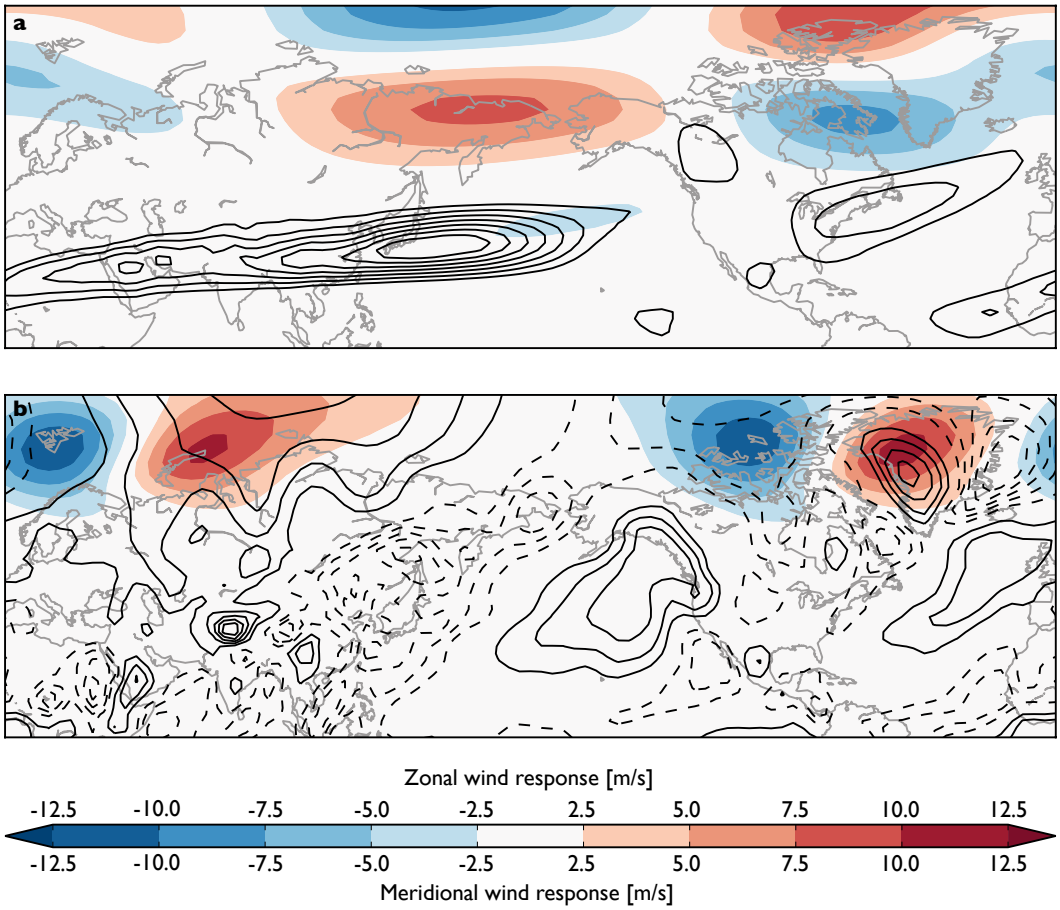

FIGURE 5.2: (a) Zonal wind response in colors, jet stream from control in contours at $\sigma = 0.257$. Contouring for jet starts at 30 m/s with an interval of 10 m/s. (b) Meridional wind response in colors, meridional wind from control in contours (negative values dashed) at $\sigma = 0.935$. Contour interval as colorbar.

Stationary heat and momentum fluxes are calculated and show in figure 5.3. These metrics provide a measure of the effect of our perturbations on the poleward transport of heat and momentum. The stationary heat flux response is only evident north of 60°N (figure 5.3 (a)). The upper level response is weak, while the lower tropospheric response is of climatological magnitude. This is to no surprise as the anomalous heating was imposed at the lower levels. The stationary momentum flux response show increase in equatorward momentum fluxes as response to anomalous Arctic heating (figure 5.3 (b)). One of the features is the weakening of the upper-level poleward stationary momentum flux at approximately 50-55°N. There is also an equatorward momentum flux response at 70°N over where the heating was imposed. Both the strongest heat- and momentum flux responses are at approximately at the same latitude. This is probably due to this area being subjected to the largest changes in baroclinicity through changes in wind shear and static stability.

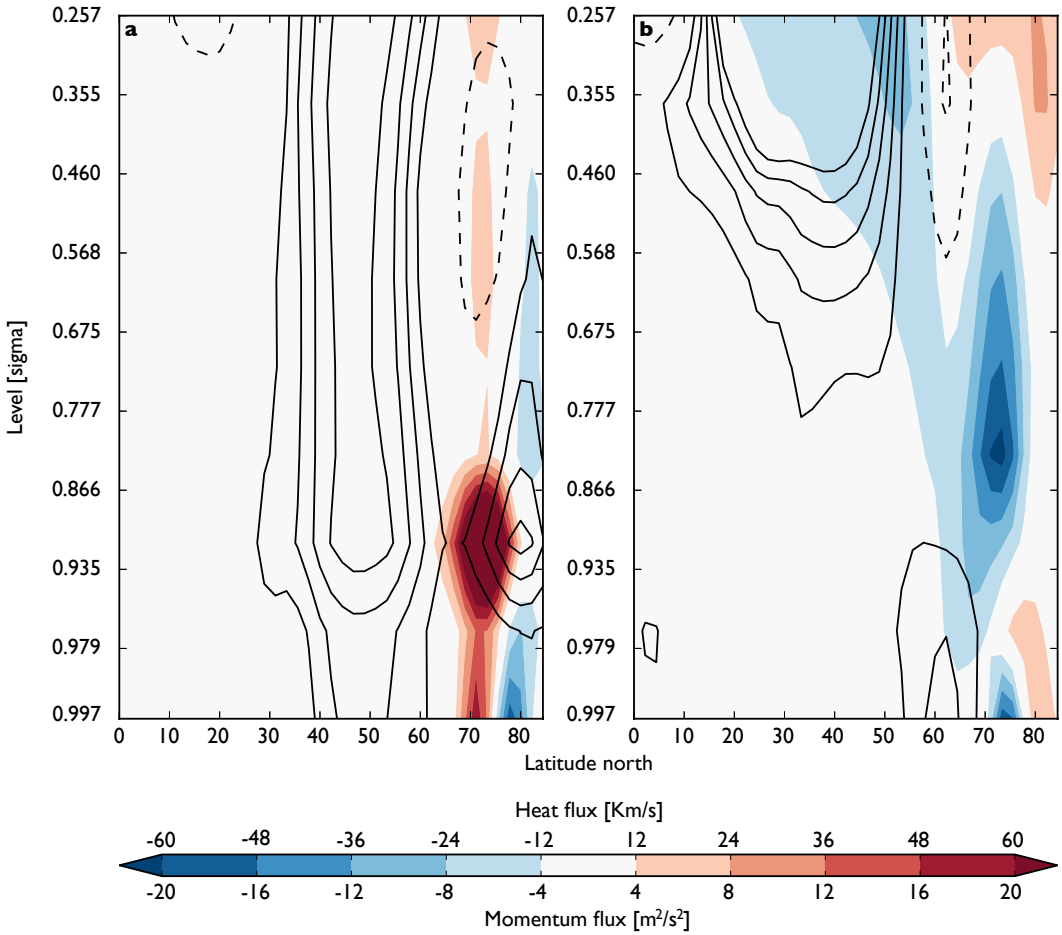

FIGURE 5.3: (a) Zonal mean of the stationary heat flux, response in colors and control in contours (negative values dashed). Same contour interval as the response. (b) Zonal mean of stationary momentum flux, response in colors and control in contours (negative values dashed). Contour interval of 10 m^2/s^2.

There are also changes in the meridional circulation index (MCI) in certain Arctic regions (figure 5.4). The MCI is a dimensionless number between -1 and 1, where -1 is a purely southward flow and 1 is a purely northward flow while 0 gives a purely zonal flow. Due to this, the MCI gives an indication of how wavy the flow is. There are three ways to change the MCI: the meridional winds strengthen, the zonal winds reduce, or a combination of these. Here, the absolute value of the MCI from climatology is subtracted from the absolute value of the MCI response, thus positive values indicates a more wavy flow while negative values indicate a less wavy flow. There is a tendency for the flow to become more wavy north of 70°N over the Canadian Archipelago and over the far East Asia region, in both regions where the upper level stationary wave patterns change in response to Arctic anomalous heating. A less wavy flow can be found in the Bering Strait. None of these regions are close to the jet stream.

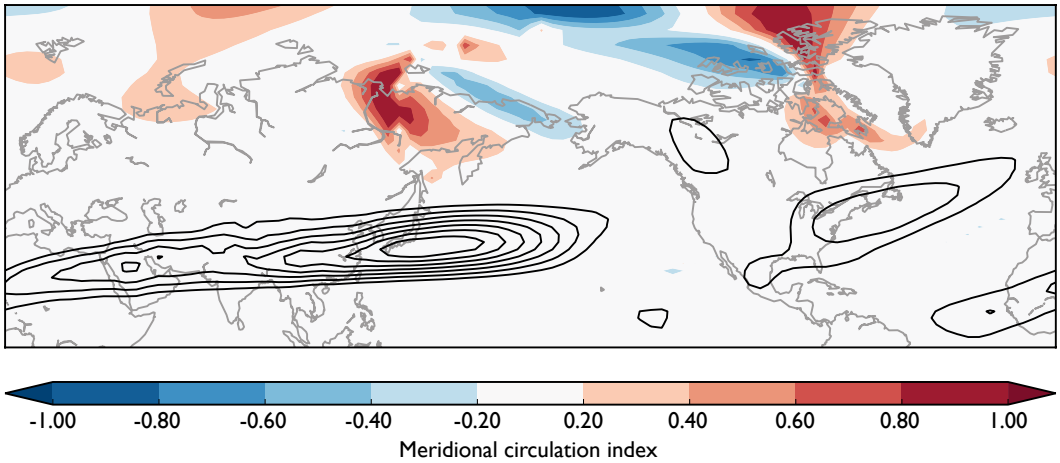

FIGURE 5.4: The absolute value response of MCI in colors, jet stream (full) from BASIC in contours at $\sigma = 0.257$. Contours starts at 30 m/s with intervals of 10 m/s.

5.2 TGR

The reduced equator-to-pole lower tropospheric temperature gradient with the nonlinear effects associated with this change did not contribute to the stationary wave response when compared to the AADIA experiment (root mean square difference between TGR and AADIA was very close to zero). This indicates that the equator-to-pole temperature gradient reduction has not been large enough during the AA period, or that this mechanism itself is not sufficient to drive a stationary wave response.

5.3 ARC and GLO

When testing the sensitivity to choice in basic state to investigate the possible effects of preconditioning, we find that a midlatitude response is detectable (figures 5.5 and 5.6). This shows that changing the basic state from climatology is sometimes sufficient enough to drive a midlatitude response. For the ARC cases, a midlatitude response appears only in certain years. On the other hand, the GLO experiments show a midlatitude response in most years, which suggests the midlatitude response depends on atmospheric variability largely outside the Arctic. Within the Arctic, the responses are similar for GLO and ARC. For both of them, the year to year stationary wave variability is large.

For the surface pressure, we examine whether ARC or GLO are able to produce NAO like patterns. First of all, the ARC surface pressure response do not extend into the midlatitudes. So its only potential contribution is through influencing the Icelandic low, but this does not seem happen. Conversely, the GLO experiments have an Icelandic

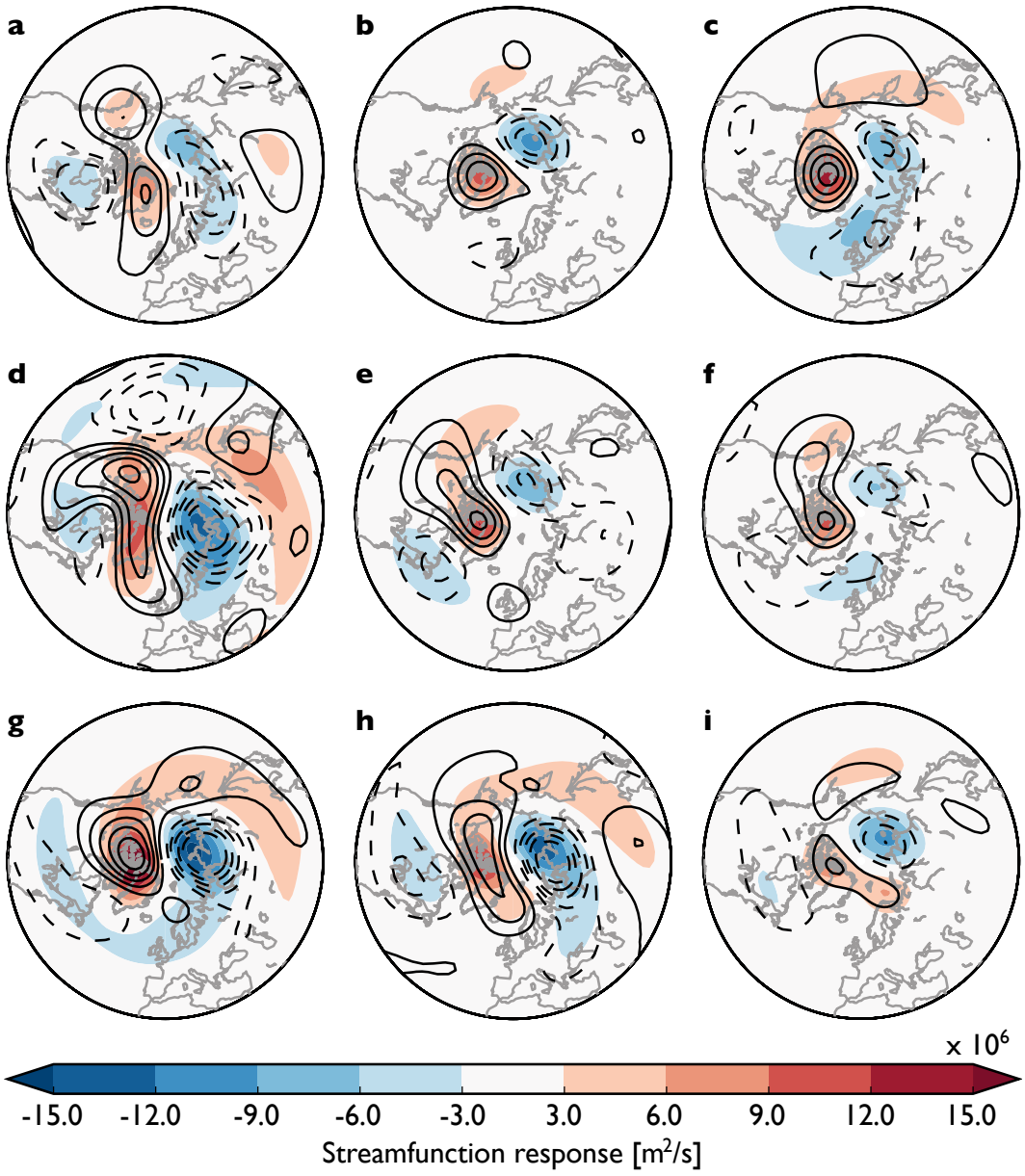

FIGURE 5.5: Streamfunction response for ARC in colors and GLO in contours (negative values dashed) at $\sigma = 0.257$. Contour interval same as coloring. For the years a) 2005-2006, b) 2006-2007, c) 2007-2008, d) 2008-2009, e) 2009-2010, f) 2010-2011, g) 2011-2012, h) 2012-2013, i) 2013-2014

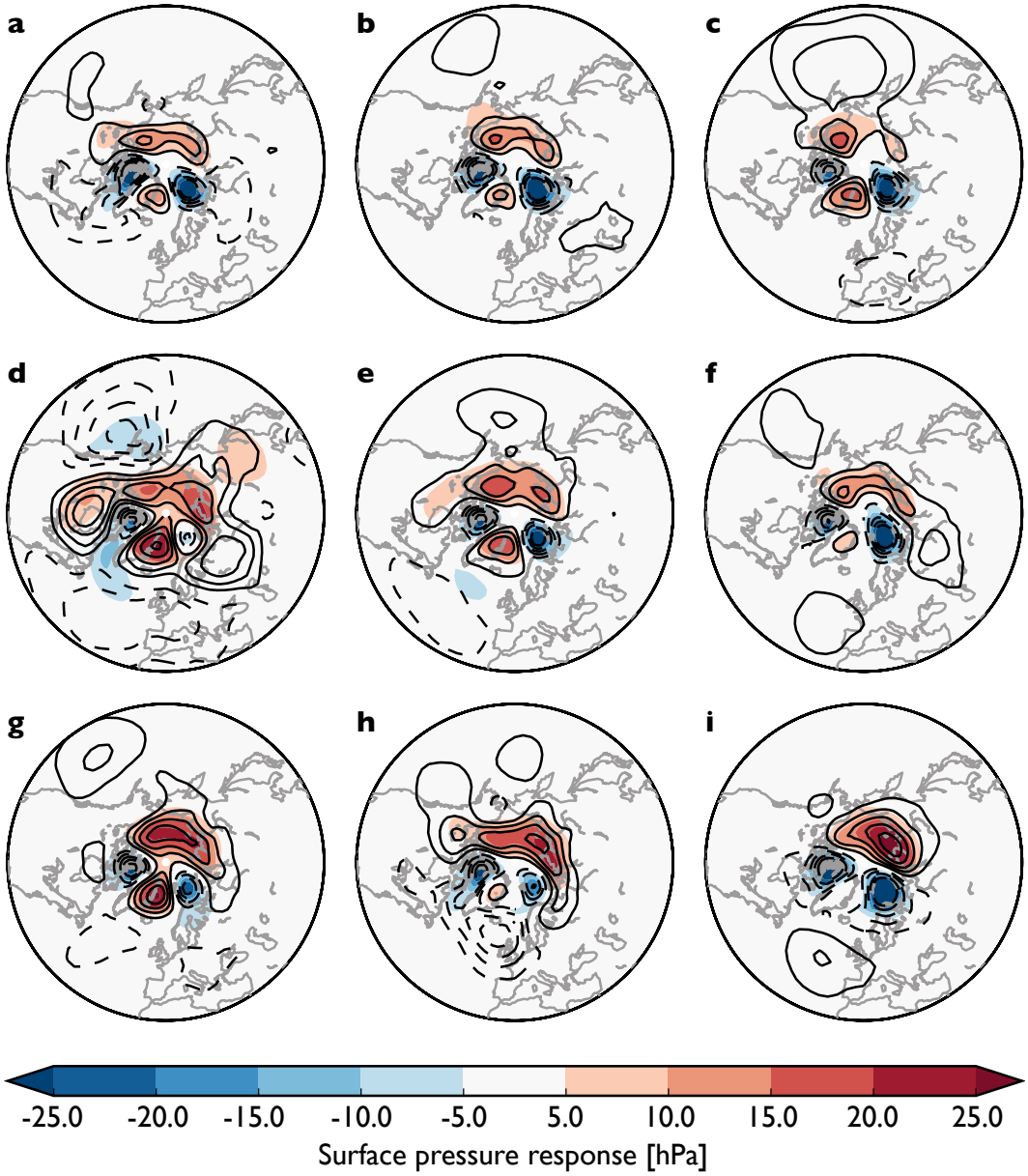

FIGURE 5.6: Surface pressure response for ARC in colors and GLO in contours (negative values dashed). Contour interval same as coloring. For the years a) 2005-2006, b) 2006-2007, c) 2007-2008, d) 2008-2009, e) 2009-2010, f) 2010-2011, g) 2011-2012, h) 2012-2013, i) 2013-2014

response in most years. This points in the direction of factors largely outside the Arctic projecting onto the NAO.

Chapter 6

Discussion and conclusions

The direct atmospheric response to heating the lower Arctic atmosphere with diabatic heating anomalies have been analyzed. The main finding is that these anomalies influence the atmospheric circulation in the Arctic at all levels but few remote changes are detected.

6.1 The midlatitude response

In this study, the most notable midlatitude response is the upper level reduction in poleward stationary wave momentum fluxes (figure 5.3 (b)). It is interesting that these stationary wave fluxes highly resemble the transient eddy driven storm track response in Butler et al. [4]. This suggests that the linear stationary wave momentum flux response to be of equal importance as the transient eddy momentum flux response in the midlatitudes.

The wavier jet stream found in Francis and Vavrus [11] claimed to be through the pathway described in Francis and Vavrus [10] cannot be explained by the heating forcing in these experiments, nor the reduced equator-to-pole temperature gradient in the lower levels. It may be that reducing the the gradient in the lower levels is insufficient for making changes in the thermally driven portion of the jet, as geostrophy and the hydrostatic approximation, which the thermal wind relation is deduced from, is only valid for the free atmosphere and not in the lower levels where turbulence and other small-scale processes dominate. This is supported by the sensitivity experiments (appendix A) which show that increasing the depth of the heating anomaly gives a stronger midlatitude response.

The NAO response reported in other studies (e.g. Alexander et al. [1], Deser et al. [9]) is not found in this study as a direct response to the heating (figure 5.1 (b)). However, these

models were nonlinear, which points towards a nonlinear interaction of the anomalous Arctic heating to be the physical mechanism linking AA to NAO. Furthermore, this response is somewhat seen in the GLO experiments (figure 5.6), which includes the effects of global internal variability. This suggest that the NAO is sensitive to internal variability and one should be careful to make conclusions on whether or not any signal is truly forced or not.

Another feature captured in other modeling studies is a wintertime equatorward shift of the jet stream as response to anomalous Arctic heating (e.g. Butler et al. [4], Seierstad and Bader [32]) which is not captured in this study. As these models are different than the linear SWM in many ways, it is hard to point to one interaction that may be the cause of the differences in their studies compared to this. One such interaction that is probably not so important is the heating and orography interaction, as Butler et al. [4]'s model did not include orography. Other nonlinear interaction of the heating anomaly, wave-mean flow interactions and internal variability are physical mechanisms which may cause the equatorward shift.

The sensitivity study in appendix A shows that a noticeable direct midlatitude response is only detected when the anomalous heating gets deeper (figure A.2). At the current state the AA-related anomalous heating is confined to the lower levels, while the upper levels are more influenced by remote circulation changes. Since the wintertime Arctic inversion layer traps the surface induced heating of the atmosphere, the way to get a deeper heating is by deepening the inversion layer. We did not investigate whether or not there has been a significant trend in the depth of the inversion layer during AA, but would recommend this for further work.

Since the AADIA heating anomalies only has a strong influence on local Arctic cicrulation, it is not unreasonable to suggest that it only has a local influence on the mean basic state as well. In the ARC experiments we showed that changes in the Arctic mean basic state also have a weak impact on midlatitude circulation. By this, it is possible to conclude that the direct impact of the realistic heating anomalies on the mean basic state can not directly drive a noticeable robust midlatitude circulation response.

6.2 The Arctic response

The baroclinic response to diabatic heating with a lowering of surface pressure where the forcing is imposed and an accompanying upper level ($\sigma = 0.257$) ridge (figure 5.1 (a)) is supported by many modeling studies (e.g. Alexander et al. [1], Deser et al. [9], Screen et al. [28]) and empirical studies also find this link (e.g. Jaiser et al. [19], Inoue

et al. [18], Hopsch et al. [17]). However, the horizontal extent found in other studies is larger and they show a pan-Arctic upper level ridge and lowering of surface pressure. The significant part of the response in these studies is contracted towards Baffin Bay and Barents-Kara seas which match well to the reported response in this study. This indicates that the response of the geopotential height to thermal forcing is fairly linear. The observational study by Hopsch et al. [17] find a very similar Arctic geopotential height pattern in February with a ridge centered over Baffin Bay/Greenland and a trough over the East Siberian Sea when comparing geopotential heights in low ice years and high ice years (where the high/low index of sea ice is based on fall sea ice extent). Since an observational study show closer resemblance to our study than sea ice forced modeling studies, it is possible to speculate whether or not sea ice forcing represents a realistic thermal forcing, or if the models generally overestimate nonlinear adjustments.

The zonal mean heat- and eddy momentum fluxes show an Arctic increase and decrease, respectively (figure 5.3). The increase of the heat flux in the Arctic lower troposphere is of opposite sign to those found in Butler et al. [4] and Seierstad and Bader [32], which points toward a nonlinear adjustment being necessary to get anomalous equatorward heat fluxes, a view shared by Jaiser et al. [19].

The MCI response (figure 5.4), which indicates if the flow is getting more meridional, does not indicate that the upper level flow is becoming more wavy as proposed by Francis and Vavrus [11] in this study. On the other hand, the meridional lower level ($\sigma = 0.935$) winds show a strengthening of the climatological winds at high latitude (figure 5.2 (b)), which would give an over all more meridional flow pattern near the surface in Arctic regions.

The conclusion for the Arctic response is that the anomalous diabatic heating related to AA has a locally high impact. However, nonlinear adjustments seems to be important. We therefore motivate to investigate nonlinear terms to understand the physical pathways better.

Appendix A

Stationary wave sensitivity to Arctic anomalous heating

The Arctic region has been subject to rapid changes during the recent AA period. While much effort has gone into understanding future projections, many aspects of the current observed changes remain unclear. The Arctic has become warmer and wetter, and will likely continue to to do so, which implies an increase in diabatic heating. However, as the chapter 3 showed, this field does not exhibit uniform changes during the AA period. Further, the sensitivity of the large-scale circulation to changes in high latititude diabatic heating is not well known. Here we examine the sensitivity of the large-scale circulation to several setups of the diabatic heating field.

A.1 Experimental setup

To investigate the atmospheric circulation's sensitivity in response to Arctic anomalous diabatic heating the stationary wave model described in chapter 4 is used. The control simulation used here is the CTRL experiment. All of the experiments carried out were based on the AADIA heating anomalies and these were perturbed in extent, magnitude, depth and location.

For any given heating anomaly, the equation is

$$\dot{Q} = V(n)H(\lambda, \phi)A \tag{A.1}$$

where $\dot{Q}$ is the diabatic heating rate, V describes the vertical structure, H describes the horizontal structure and A is the maximum magnitude. n is number of levels heating is applied to, λ is longitude and ϕ is latitude.

A.1.1 Extent

The first experiment was conducted to test the sensitivity to horizontally shrinking or expanding anomalous diabatic heating fields. The horizontal extent of the heating anomalies is given by

$$H(\lambda, \phi) = cos^2(\frac{\lambda - \lambda_0}{\Delta\lambda})cos^2(\frac{\phi - \phi_0}{\Delta\phi}) \tag{A.2}$$

where the following conditions were applied.

$$\lambda\epsilon[\lambda_0 - \Delta\lambda, \lambda_0 + \Delta\lambda] \tag{A.3}$$

$$\phi\epsilon[\phi_0 - \Delta\phi, \phi_0 + \Delta\phi] \tag{A.4}$$

Where λ and ϕ did not meet this criterion,

$$H(\lambda, \phi) = 0 \tag{A.5}$$

In this experiment, we perturbed the horizontal extent as seen in table A.1 while vertical structure and magnitude was kept as in AADIA.

A.1.2 Magnitude

This experiment was to test the sensitivity to the strength of the diabatic heating anomaly. The strength is given by A in (A.1).

In this experiment, we perturbed the magnitude from 0.5K/day to 5.0K/day while vertical structure, extent and location was kept as in AADIA.

A.1.3 Depth

Experiment	$\Delta\lambda$ [°]	Baffin Bay λ_0 [°E]	Barents λ_0 [°E]	$\Delta\phi$ [°]	ϕ_0 [°N]	Extent
1	8.0	280.0	40.0	1.5	76.5	0.047
2	16.0	280.0	40.0	3.0	76.5	0.169
3	24.0	280.0	40.0	4.5	76.5	0.263
4	32.0	280.0	40.0	6.0	76.5	0.507
5	40.0	280.0	40.0	7.5	76.5	0.825
AADIA	40.0	280.0	40.0	8.5	76.5	1.000
6	48.0	280.0	48.0	9.0	76.5	1.227
7	56.0	280.0	56.0	10.5	76.5	1.450
8	64.0	280.0	64.0	11.25	77.25	1.658
9	72.0	280.0	72.0	12.0	78.0	1.848
10	80.0	280.0	80.0	12.0	78.0	2.037
11	88.0	272.0	88.0	12.0	78.0	2.226
12	90.0	270.0	90.0	12.0	78.0	2.274

TABLE A.1: Size and placement of the Baffin Bay and Barents anomalies. Extent is scaled to the AADIA horizontal extent.

Here we test the sensitivity to the depth of the diabatic heating anomaly. The depth of the anomaly is given by

$$V(n) = \frac{V(\sigma_{k-1}) + k \cdot 2}{V(\sigma_n)} \tag{A.6}$$

where $k = 0, 1, ..., n$, n is the number of levels heating is applied to, $V(\sigma_0) = 0$ and σ_n is the level nearest surface. The magnitude, horizontal extent and location was as in AADIA. For the AADIA experiment, $n = 0$.

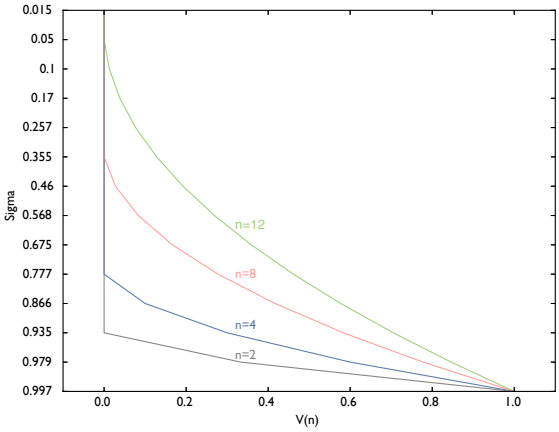

FIGURE A.1: The vertical structure of the heating anomaly with varying n.

A.1.4 Location

This experiment was carried out to test if the stationary wave response was sensitive to the location of the heating anomaly. It was done by varying λ_0 and ϕ_0 from equation (A.2) as seen in table A.2. Only one heating anomaly was applied per experiment with fixed $\Delta\lambda = 40°$ and $\Delta\phi = 8.5°$.

Experiment	λ_0 [°E]	ϕ_0 [°N]
Barents	40	76.5
Kara	90	76.5
East Siberian	150	76.5
Beaufort	210	76.5
Canadian archipelagos	270	76.5
Greenland	320	76.5
Barents N	40	81.5
Kara N	90	81.5
East Siberian N	150	81.5
Beaufort N	210	81.5
Candian archipelagos N	270	81.5
Greenland N	320	81.5

TABLE A.2: Placement of heating anomalies

A.2 Results and discussion

The stationary wave response increases with increasing horizontal extent, up to an infliction point whereafter the response decrease (figure A.2 a). This show that there is an optimal choice of extent for triggering a stationary wave response, connected to the Rossby radius of deformation. With a declining sea ice extent during AA, it is not unrealistic to expect that the diabatic heating anomalies will expand and thereby create stronger changes in the midlatitude circulation. However, the maximum strength of the response is only 52.8% stronger compared to the already weak response the AADIA anomalies gave.

The relationship between the magnitude of the heating anomaly and the stationary wave response is not one-to-one (figure A.2 b). The response increase at first and peaks when the heating anomaly is prescribed with a magnitude of 1.0 K/day. This might be due to the climatological diabatic heating being close to 1.0 K/day in these regions, so the stationary waves responds strongly to a shift of sign in the diabatic heating. When the heating anomaly is further strengthened the stationary wave response decrease and seems to converge towards a maximum amplitude of approximately 10% of the maximum amplitude of the climatological waves. Since the SSTs have significantly increased in winter during the AA it is not unexpected that it will continue to increase. This may cause the diabatic heating anomalies, which are already at 1.5 K/day at maximum, to strengthen. Due to this, it is not unrealistic to expect the strength of the midlatitude stationary wave response to decrease.

The relationship between the depth of the heating anomaly and the response of the waves is close to one-to-one (figure A.2 c). There response is very weak when heating is applied at the three lowest levels, but when applied to the fourth lowest level ($\sigma = 0.866$)

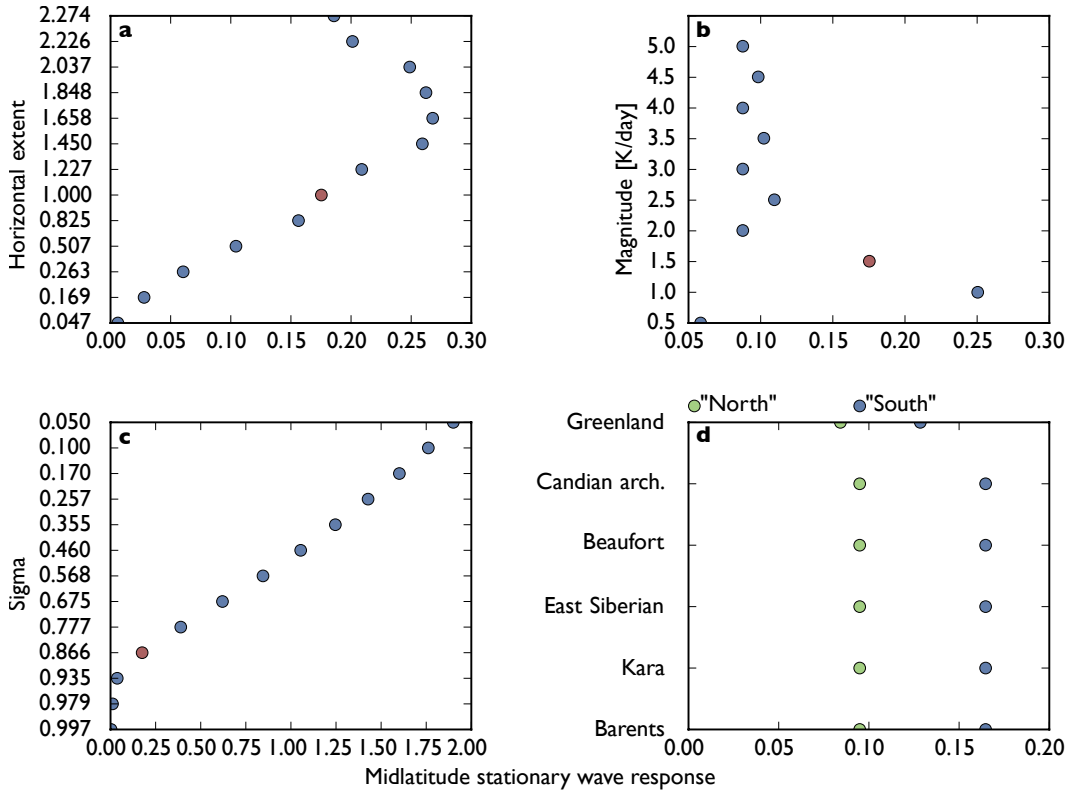

FIGURE A.2: The midlatitude stationary wave response at $\sigma = 0.257$ to (a) extent, (b) magnitude, (c) depth and (d) location of diabatic heating anomalies. Midlatitude is defined as 30°N-60°N, and the response was scaled with $30 \cdot 10^6$ m^2/s which is the maximum amplitude of the climatological stationary waves in midlatitudes. The red dot indicates the AADIA experiment.

as well, a response is detectable. This is probably due to the fourth level being very close to the top of the Arctic boundary inversion layer. The stationary wave response is as strong as the climatological waves when heating is applied up to $\sigma = 0.460$ and further increase when the heating anomaly gets deeper. However, the wintertime heating anomaly's vertical structure is dependent on the depth of the inversion layer as heating is trapped underneath (Screen et al. [29]).

The stationary wave response is little sensitive to the location of the heating anomalies (figure A.2 d). For the "north" and "south" experiments all the locations give the same response except for Greenland where the response is somewhat weaker. In a nonlinear model this could be understood through the interaction between the anomalies and Greenland's orography. However, this is not a nonlinear model and it is hard to assess why this location provides a weakening of the wave response. Generally the "north" experiments are weaker than the "south" experiments which is to no surprise as the "south" anomalies are closer to the midlatitudes.

The pattern of the midlatitude stationary wave response is not sensitive to extent, depth,

magnitude or location. When all experiments are scaled in a manner that gives the maximum midlatitude response to be 1 for each of the experiments (for the anomalies that has different center than AADIA, the response was shifted longitudinally/latitudinally accordingly), the root mean square difference in the midlatitudes is close to zero for the depth and extent experiments, while zero for the location and magnitude experiments.

Bibliography

[1] Alexander, M. A., Bhatt, U. S., Walsh, J. E., Timlin, M. S., Miller, J. S., and Scott, J. D. (2004). The atmospheric response to realistic arctic sea ice anomalies in an agcm during winter. *Journal of Climate*, 17(5):890–905.

[2] Barnes, E. A. (2013). Revisiting the evidence linking arctic amplification to extreme weather in midlatitudes. *Geophysical Research Letters*, 40(17):4734–4739.

[3] Brown, R., Derksen, C., and Wang, L. (2010). A multi-data set analysis of variability and change in arctic spring snow cover extent, 1967–2008. *Journal of Geophysical Research: Atmospheres*, 115(D16):n/a–n/a. D16111.

[4] Butler, A. H., Thompson, D. W. J., and Heikes, R. (2010). The steady-state atmospheric circulation response to climate change–like thermal forcings in a simple general circulation model. *Journal of Climate*, 23(13):3474–3496.

[5] Chan, S. C. and Nigam, S. (2009). Residual diagnosis of diabatic heating from era-40 and ncep reanalyses: Intercomparisons with trmm. *Journal of Climate*, 22(2):414–428.

[6] Cohen, J., Screen, J. A., Furtado, J. C., Barlow, M., Whittleston, D., Coumou, D., Francis, J., Dethloff, K., Entekhabi, D., Overland, J., and Jones, J. (2014). Recent arctic amplification and extreme mid-latitude weather. *Nature Geosci*, 7(9):627–637.

[7] Cohen, J. L., Furtado, J. C., Barlow, M. A., Alexeev, V. A., and Cherry, J. E. (2012). Arctic warming, increasing snow cover and widespread boreal winter cooling. *Environmental Research Letters*, 7(1):014007.

[8] Coumou, D. and Rahmstorf, S. (2012). A decade of weather extremes. *Nature Clim. Change*, 2(7):491–496.

[9] Deser, C., Tomas, R., Alexander, M., and Lawrence, D. (2010). The seasonal atmospheric response to projected arctic sea ice loss in the late twenty-first century. *Journal of Climate*, 23(2):333–351.

[10] Francis, J. A. and Vavrus, S. J. (2012). Evidence linking arctic amplification to extreme weather in mid-latitudes. *Geophysical Research Letters*, 39(6):n/a–n/a.

[11] Francis, J. A. and Vavrus, S. J. (2015). Evidence for a wavier jet stream in response to rapid arctic warming. *Environmental Research Letters*, 10(1):014005.

[12] Hall, A. (2004). The role of surface albedo feedback in climate. *Journal of Climate*, 17(7):1550–1568.

[13] Hartmann, D., Tank, A. K., Rusticucci, M., Alexander, L., Brönnimann, S., Charabi, Y., Dentener, F., Dlugokencky, E., Easterling, D., Kaplan, A., Soden, B., Thorne, P., Wild, M., and Zhai, P. (2013). *Observations: Atmosphere and Surface. In: Climate Change 2013: The Physical Science Basis. Contribution of Working Group I to the Fifth Assessment Report of the Intergovernmental Panel on Climate Change*, pages 159–254. Cambridge University Press, Cambridge, United Kingdom and New York, NY, USA.

[14] Held, I. M., Ting, M., and Wang, H. (2002). Northern winter stationary waves: Theory and modeling. *Journal of Climate*, 15(16):2125–2144.

[15] Holton, J. (2004). *An Introduction to Dynamic Meteorology*. Number vol. 1 in An Introduction to Dynamic Meteorology. Elsevier Academic Press.

[16] Honda, M., Inoue, J., and Yamane, S. (2009). Influence of low arctic sea-ice minima on anomalously cold eurasian winters. *Geophysical Research Letters*, 36(8):n/a–n/a. L08707.

[17] Hopsch, S., Cohen, J., and Dethloff, K. (2012). Analysis of a link between fall arctic sea ice concentration and atmospheric patterns in the following winter. *Tellus A*, 64(0).

[18] Inoue, J., Hori, M. E., and Takaya, K. (2012). The role of barents sea ice in the wintertime cyclone track and emergence of a warm-arctic cold-siberian anomaly. *Journal of Climate*, 25(7):2561–2568.

[19] Jaiser, R., Dethloff, K., Handorf, D., Rinke, A., and Cohen, J. (2012). Impact of sea ice cover changes on the northern hemisphere atmospheric winter circulation. *Tellus A*, 64(0).

[20] James, I. (1995). *Introduction to Circulating Atmospheres*. Cambridge Atmospheric and Space Science Series. Cambridge University Press.

[21] Kalnay, E., Kanamitsu, M., Kistler, R., Collins, W., Deaven, D., Gandin, L., Iredell, M., Saha, S., White, G., Woollen, J., et al. (1996). The ncep/ncar 40-year reanalysis project. *Bulletin of the American meteorological Society*, 77(3):437–471.

[22] Ling, J. and Zhang, C. (2012). Diabatic heating profiles in recent global reanalyses. *Journal of Climate*, 26(10):3307–3325.

[23] Liu, J., Curry, J. A., Wang, H., Song, M., and Horton, R. M. (2012). Impact of declining arctic sea ice on winter snowfall. *Proceedings of the National Academy of Sciences*, 109(11):4074–4079.

[24] Outten, S. D. and Esau, I. (2012). A link between arctic sea ice and recent cooling trends over eurasia. 110(3-4):1069–1075.

[25] Parkinson, C. L. and Comiso, J. C. (2013). On the 2012 record low arctic sea ice cover: Combined impact of preconditioning and an august storm. *Geophysical Research Letters*, 40(7):1356–1361.

[26] Pithan, F. and Mauritsen, T. (2014). Arctic amplification dominated by temperature feedbacks in contemporary climate models. *Nature Geosci*, 7(3):181–184.

[27] Ringler, T. D. and Cook, K. H. (1999). Understanding the seasonality of orographically forced stationary waves: Interaction between mechanical and thermal forcing. *Journal of the Atmospheric Sciences*, 56(9):1154–1174.

[28] Screen, J., Deser, C., Simmonds, I., and Tomas, R. (2014). Atmospheric impacts of arctic sea-ice loss, 1979–2009: separating forced change from atmospheric internal variability. 43(1-2):333–344.

[29] Screen, J. A., Deser, C., and Simmonds, I. (2012). Local and remote controls on observed arctic warming. *Geophysical Research Letters*, 39(10):n/a–n/a. L10709.

[30] Screen, J. A. and Simmonds, I. (2010). The central role of diminishing sea ice in recent arctic temperature amplification. *Nature*, 464(7293):1334–1337.

[31] Screen, J. A. and Simmonds, I. (2013). Exploring links between arctic amplification and mid-latitude weather. *Geophysical Research Letters*, 40(5):959–964.

[32] Seierstad, I. and Bader, J. (2009). Impact of a projected future arctic sea ice reduction on extratropical storminess and the nao. 33(7-8):937–943.

[33] Simmonds, I. and Rudeva, I. (2012). The great arctic cyclone of august 2012. *Geophysical Research Letters*, 39(23):n/a–n/a. L23709.

[34] Sobolowski, S., Gong, G., and Ting, M. (2010). Investigating the linear and nonlinear stationary wave response to anomalous north american snow cover. *Journal of the Atmospheric Sciences*, 68(4):904–917.

[35] Taylor, P. C., Cai, M., Hu, A., Meehl, J., Washington, W., and Zhang, G. J. (2013). A decomposition of feedback contributions to polar warming amplification. *Journal of Climate*, 26(18):7023–7043.

[36] Ting, M. (1994). Maintenance of northern summer stationary waves in a gcm. *Journal of the Atmospheric Sciences*, 51(22):3286–3308.

[37] Ting, M. (1996). Steady linear response to tropical heating in barotropic and baroclinic models. *Journal of the Atmospheric Sciences*, 53(12):1698–1709.

[38] Wallace, J. M., Held, I. M., Thompson, D. W. J., Trenberth, K. E., and Walsh, J. E. (2014). Global warming and winter weather. *Science*, 343(6172):729–730.

[39] Wang, H. and Ting, M. (1999). Seasonal cycle of the climatological stationary waves in the ncep–ncar reanalysis. *Journal of the Atmospheric Sciences*, 56(22):3892–3919.